Electroactive Covalent Organic Frameworks: Design, Synthesis, and Applications

Yusran Q Yusran, Qianrong Fang, Valentin Valtchev

WILEY-VCH

Electroactive Covalent Organic Frameworks: Design Synthesis and Applications

Yusran Yusran, Qianrong Fang* and Valentin Valtchev

Y. Yusran, Prof. Q. Fang

State Key Laboratory of Inorganic Synthesis and Preparative Chemistry, Jilin University, Changchun 130012, P. R. China

E-mail: qrfang@jlu.edu.cn

Prof. V. Valtchev

Normandie Université, ENSICAEN, UNICAEN, CNRS, Laboratoire Catalyse et Spectrochimie, 14000 Caen, France

Abstract: Covalent organic frameworks (COFs) are an emerging class of crystalline porous polymers with tailorable compositions, porosities, functionalities and profound chemical stability. The manageable installation of electroactive moieties on the skeletons and pore walls of COFs transforms them into promising electroactive materials that are applicable for energy-related applications. Significant progresses have been made in the application of electroactive COFs for electrochemical energy storages and conversions. Herein, the recent advances in the design and application of electroactive COFs in capacitors, batteries, conductors, fuel-cells, water-splitting, and electrocatalysis are presented. Their remarkable performances are discussed and compared with other porous materials, while perspectives in development of electroactive COFs are also provided.

Keywords: covalent organic frameworks (COFs), electroactive materials, energy storages, energy conversions

1. Introduction

The huge demand and consumption of energy in our global society have led to the scarcity of traditional energy sources and have caused serious challenges to energy supplies and environmental protection. Exploration of other energy sources which are renewable, abundant, economic and technologically greener is emergent and important. In addition, the huge energy resources in our planet, such as sunlight, fossil fuels, winds, hydro/geothermal, and nuclear powers, which can be transformed via suitable devices into electricity, should be stored safely in efficient ways.[1,2] Indeed, storing electricity is important for portable energy supply. In practical, the high efficiency, sustainability and pollution-less of capacitors or batteries for energy storage, electrochemical water splitting for hydrogen production, and fuel-cells for electricity generation, have been dictated as prospective solutions to well-preserve and transform and also to eradicate our dependence on traditional fossil energy.[2–4] Currently, these emerging technologies are under intensive R&D, in which water splitting is believed to be pivotal technology for efficient sustainable energy generation along with batteries and fuel cells as promising energy storage devices.[1,5] However, despite their potential utilization, those technologies are generally costly and require electroactive noble metals such as Pt and RuO_2 to induce the key electrochemical reactions, such as oxygen reduction reaction (ORR), oxygen evolution reaction (OER) and hydrogen evolution reaction (HER).[1,6]

In their developments, extensive efforts and rapid progresses in the research of electroactive materials have involved porous materials[7], such as amorphous porous organic polymers (POPs) and their derivatives[8–10], porous carbons[11], crystalline inorganic zeolites[12–14], and even with metal-organic frameworks (MOFs) compounds.[15–17] Those porous materials not only demonstrated an impressive confinement toward electroactive species but also possessed electroactive components in their frameworks, thus their pristine compounds are somehow electroactive. For example, MOFs are basically composed of

various type of transition metals and organic linkers that are electrochemically active.[18,19] Meanwhile, high surface area MOFs are perfect host to accommodate electroactive metals and other electroactive molecules[20–22], thus electroactive hybrid materials are systematically obtained. Recently, another type of crystalline porous polymer that are made by lightweight organic elements have been discovered, namely covalent organic frameworks (COFs).[23] COFs are crystalline and highly porous polymers in which their building units are connected by strong covalent bonds and precisely integrated into an extended structure with periodical skeleton and ordered pores.[24–26] Compared to zeolites, MOFs and COFs exhibit relatively higher surface areas, lower densities and profound chemical stabilities.[27] In addition, the synthesis of COFs allow for tailorable compositions and functionalities via predesigned building blocks or post-synthetic modification of the established frameworks.[28–30] This synthesis advantage includes the manageable installation of electroactive moieties on the skeletons and pore walls of COF, thus transforms them into prospective electroactive materials that are applicable for energy-related applications.[31–33]

Although the research of COFs is still infancy, several electroactive COFs have been designed and explored for energy-related applications. For example, 2D and 3D COFs have been employed as promising electrochemical double layer capacitor (EDLC) electrodes[34] and electrical conductors.[35] In addition, in the field of batteries, electrocatalysis, and fuel cells, COFs have also appeared recently.[36–38] In this review paper, the recent progress of design synthesis of electroactive COFs and their applications in the field of electrochemical energy storages and conversions, and in electrocatalysis are overviewed. Their performances in the field of capacitor, battery, conductor, fuel-cell, and electrocatalysis are discussed and perspectives on developing electroactive COFs as future smart materials for energy storages and conversions are provided.

2. Design Principles of Electroactive COFs

To enable COFs to conduct both ions and electrical charges or store electrochemical energy in capacitors and batteries, specific design of COFs with electroactive sites is critical. Similarly, to execute electrocatalytic phenomena in key electrochemical reactions (e.g., ORR, OER and HER), COF-based electrocatalysts should possess catalytic sites which are able to undertake efficient catalytic processes and avoid overpotential.[39] Thus, careful design of electroactive COFs with abundant accessible active sites, long-term durability and if possible, low-cost and greener technologies is pivotal. The design of electroactive COFs has been performed in various strategies, including preparing COFs with high surface areas and accessible active surfaces, incorporating electroactive sites (e.g., electron-rich species and metals) on their frameworks, and hybridizing COFs with other electroactive components to enhance their electroactivity. To make these more practical, we provide a scheme (**Scheme 1**) to describe how electroactive COFs were designed so far and further discuss them in the following sub-sections.

2.1. Electroactive Bulk and Exfoliated COFs

The accessible surface areas and active sites in porous materials can directly influence their activities. Similarly, the design of electroactive COFs also takes the aforementioned consideration into account. Particularly, the bulk and exfoliated COFs are two types of COFs that are morphologically distinct and provide different accessibility toward their electroactive sites (**Scheme 1**a). Generally, COFs were prepared as bulk-crystalline powder and haven been widely employed in various kind of applications.[40–43] Meanwhile, several efforts such as preparing bulk-COFs with controlled pore size have also been done to produce high surface areas and to drive for more accessibility of the active sites. This tailorable synthesis is judiciously performed by utilizing building blocks with varied length and dimension. For example, Jiang and team prepared a high surface area mesoporous 2D imide-linked D_{TP}-A_{NDI}-COF with a pore size of 5.06 nm for construction of Li-ion battery electrode[44], while Li and

co-workers reported another 2D imide-linked PIBN based COF with pore size of 1.4 nm for similar application.[45] These two electroactive COFs with distinct porosity exhibited remarkable and unique performances in the field of battery. In addition, COFs have also been prepared as bulk thin films or membranes. For example, Halder *et al*. synthesized flexible, self-standing and chemically stable thick sheet (~200 μm) TpOMe-DAQ COF as high performance pseudocapacitor.[40] This typical example of design bulk COFs exemplifies the robust design of COFs as promising electroactive materials.

Beside as bulk-crystalline powder, exfoliating or delaminating the layer structure of 2D electroactive COFs has recently been a steaming research to enhance the accessibility of the active sites and reduce the layer aggregation. For instance, Yusran *et al.* exfoliated porphyrin-based mesoporous 2D COFs to obtain few-layer exfoliated COFs (e-COFs) that were able to store electrical charges at high scan rate.[34] With similar vision, another 2D COF was exfoliated by ball-milling method to produce much more thinner exfoliated COF (e-COF).[46] Furthermore, the obtained e-COF was employed as cathode in Li-ion batteries (LIBs). This synthetic procedure clearly demonstrated enhancement of electroactivity of the COF since exfoliation could lead for the exposition of active site into high extent.

2.2. Electroactive COFs with Reactive Skeletons

Installing electroactive components into the COF skeleton is one of the straightway approach to design electroactive COFs (**Scheme 1**b). Such effort can directly be done by employing building blocks with electroactive backbones. Specifically, the electroactive sites can be existed as linkages or tether on the backbones of COFs. For instance, several electroactive COFs with electron rich heteroatoms (e.g., S, N and O) have been designed. Meanwhile, COFs with ionic or charged skeletons have also been prepared and they may show electroactivity.

For example, bottom-up design of electroactive COF (Tp-Azo) was reported by installing electron rich-azo (-N=N-) groups on its skeleton that were originated form its building block.[47] Since azo groups can stabilize H_3PO_4 once protonated[48], H_3PO_4 doped Tp-Azo was a perfect material for proton conductor application. Under similar scenario, another COF was bottom-up designed by condensing tetraaminophenone and cyclohexanehexaone building blocks to give COF (TQBQ-COF) with electron-rich nitrogen on its linkages and carbonyl groups on its skeleton.[49] The presence of abundant N atoms on the skeleton reduced the electronic band gap and enhanced the electronic conductivity. Indeed, TQBQ-COF exhibited high capacity in sodium-ion batteries (SIBs). Similarly, electroactive COFs can also be prepared by bottom-up installing ionic or charge species on their skeleton. For instance, ionic-COFs (ICOFs) were designed by condensing hydroxyl-based macrocycle building block with trimethyl borate affording COF with anionic spiroborate linkages.[50] More importantly, the ionic sites could be counter balanced with lithium ions, hence ICOFs were potential for ionic conductor application. Meanwhile, electroactive COFs with cationic skeleton has also been designed, exemplifying the robust design of electroactive COF with ionic skeleton.[51]

2.3. Electroactive COFs with Reactive Functional Groups

Decoration of functional groups in COFs is very facile and has been widely demonstrated.[28–30,52,53] This synthesis platform includes the manageable installation of reactive functional groups on the frameworks to produce electroactive COFs (**Scheme 1**c). Wide range of reactive functional groups have been installed in COFs, such as functional groups that contained electron-rich, ionic or charged species. Technically, this type of COFs can be prepared via either bottom-up approach (by condensing building blocks completed with reactive functional groups) or postsynthetic functionalization of the established frameworks with reactive functional groups.

Through bottom-up approaches, several COFs with reactive functional groups have been designed. For example, sulfonated 2D COF (NUS-10) was prepared by condensing sulfonated building blocks.[54] Indeed, the resultant NUS-10 exhibited intrinsic proton conductivity which was influenced by the presence of the sulfone functional groups. Similarly, to obtain COFs with oxygen-rich poly(ethylene oxide) (PEO) (COF-PEO-*x*, *x* = 3, 6 or 9) chains, one way was reported by condensing PEO-based building units with different length of PEO chains (**Figure 1**a).[55] Accordingly, since bulky PEO chains can solvate Li^+ for fast transport by its segmental motion[56,57], COF-PEO-*x* series were perfect materials for Li-ion conductor. Furthermore, the design of this type of electroactive COFs could also be performed under two-steps postsynthetic methods. For instance, the design of electroactive COF-F-S was executed by chemically modifying the pre-established fluoride-based COF (COF-F) with elemental polysulfur (PS) (**Figure 1**b).[41] Interestingly, COF-F-S demonstrated high electrical capacity compared to COF-F when used as cathode in Li-S batteries. The robust design of electroactive COFs by introducing reactive functional groups promises the great prospective in developing COF materials for energy-related applications.

2.4. Electroactive COFs with Reactive Metals

Generally, transition-metals are redox-active. Thus, electroactive COFs can be designed by introducing those metals into their frameworks. Practically, metals can either be settled on the skeleton or tethered on the pore surface of COFs with coordinative sites (**Scheme 1**d). In addition, the design of such electroactive COFs can be executed in both bottom-up and postsynthetic approaches.

For example, in 2015, Yaghi and team bottom-up designed COFs with metals (COF-366-Co and COF-367-Co/Cu) by condensing metallated-porphyrin monomer with corresponding linear building blocks.[37] The COFs were composed of electroactive metals (Co and Cu) situated on the porphyrin moieties. Meanwhile, by designing coordinative sites on skeleton,

electroactive metals can facilely be installed on the COFs under postsynthetic approach. For example, Banerjee and team designed hydroquinone-based HqTp COF as perfect host to hold Zn^{2+} ions as promising material for aqueous rechargeable zinc-ion batteries (ZIBs).[58] Structurally, HqTp COF possessed C=O and N–H coordinative sites that are capable of coordinating Zn^{2+} ions in an electrochemical cell.[59,60] Hence, after Zn^{2+} ions intercalation, Zn/HqTp COF-based cell exhibited notable discharge capacity at destined voltage. These two reported works demonstrated the robust design of electroactive COFs by introduction of redox-active metals.

2.5. Electroactive COF Hybrids

Beside with electroactive skeletons, functional groups and metals, another attempt to design electroactive COFs is by hybridizing or composing COFs with electroactive components (**Scheme 1**e). Several materials such as porous carbons (e.g., conductive carbon, graphene, graphite and CNTs)[61], organic polymers (e.g., polyaniline and polypyrrole)[62–64] and inorganic molecules (e.g., polysulfide)[65,66] are electroactive. Thus, they are able to enhance the electroactivity of COFs by hybridizing them with COFs. Beside their high conductivity and redox activities, these materials are somehow compatible with COFs by specific material design.

Several COF hybrids composed of conductive and redox active materials have been reported. For example, a 2D imine-linked COF with few layers architecture was deposited on surface of CNTs to obtain COF@CNTs as active material for LIBs electrode.[67] The successful deposition of the COF onto CNTs was due to π–π interaction between these two components. Interestingly, the resultant COF@CNTs demonstrated large Li-ion capacity compared to bulk COF which were assumed as synergetic effect between two components. Furthermore, redox-active inorganic molecules such as polysulfide could also be deposited on the pore of COFs to enhance the lithium storage of bare COFs. For instance, the thermal

deposition of sulfur molecules into the pore of COF-1 to produce COF-1/S composite enhanced the lithium capacity COF in LIBs.[68] These representative works demonstrate the wide range of material designs in preparing electroactive COF hybrids with unique and remarkable electroactivity.

3. Applications of Electroactive COFs

The manageable incorporation of electroactive constituents in COFs promises abundant applications in the electrical-related fields. In addition, COFs provide large surface areas to confine the interest molecules and control the accessible exposed active sites. Meanwhile, their high chemical and thermal stabilities, ensure the structural and active sites preservation and adaptability for performing chemical reactions even at harsh conditions. All these properties call for great potential utilization of electroactive COFs in the field of electrochemical energy storages (e.g., capacitors and batteries), electrochemical energy generation (e.g., ORR, OER, HER and fuel-cells), electrical/ionic conductors and electrocatalysis.

3.1. Electroactive COFs for Capacitors

Electrochemical energy storages are emerging devices for mobile electrical energy supplies.[69] The widely known of batteries and capacitors are the most explored devices with various kinds of materials have been utilized as active materials and varied fabrication techniques.[70] Compared to batteries, capacitors are particularly interesting due to their high power density, fast charge-discharge rates and long-life span.[71] Typically, construction of capacitor utilizes highly conductive, thermal and chemically stable, and yet highly porous materials. Meanwhile, according to their electrical energy storage mechanisms, capacitor devices are divided into two types; electrochemical double-layer capacitors (EDLCs) and pseudocapacitors.[72] The EDLCs store electrical energy via electrostatic accumulation of charges at the electrode-electrolyte interface, while supercapacitors involve electrosorption

and/or reversible redox reactions at or near the surface of the electrode materials. The high porosity, discrete pore size and tunable redox active sites installation in COFs, made these materials promise as active components for capacitor construction. So far, COFs have been designed and employed as active materials for both EDLCs and pseudocapacitors electrodes constructions.

3.1.1. Electrochemical Double-Layer Capacitors (EDLCs)

Since EDLCs store electrical charge without involving chemical reaction (e.g., redox-reaction), porous materials with high conductivity and high surface area are indispensable for EDCL electrode construction. Hence, as highly porous materials, COFs hold great potential as active materials for EDLC electrodes.

Recently, Yusran *et al.,* reported a design of highly stable mesoporous 2D porphyrin-based COFs (termed JUC-510, JUC-511, JUC-512; JUC= Jilin University) as active materials for EDLC electrodes (**Figure 2**).[34] The high surface areas (up to 1170 m^2 g^{-1}), mesoporous pores (3.4 nm) and the presence of electroactive and conductive metallated-porphyrin in JUC-COFs, induced capacitance capabilities of the COFs. To ensure the efficient charges mobility and double-layer storage, the COFs were further exfoliated to obtain a few layer thin-sheet COFs (e-COFs). Interestingly, the e-COF based capacitors were not only able to demonstrate efficient double-layer charge storage but also showed retention storage capability at significantly high scan rate (up to 30,000 mV s^{-1}), a common performance found in microcapacitor-type capacitors.[73,74] Furthermore, they exhibited high areal capacitances (e.g., 5.46 mF cm^{-2} at 1,000 mV s^{-1}) and high gravimetric power (55 kW kg^{-1}), that were superior to microcapacitor and conventional graphitic carbon capacitors. These remarkable capacitance performances arose from the well-defined a few layer architectures with large pore size and the chemically stable of e-COFs as active materials. Such systematic design of electroactive COFs could herald the exploration of COFs as promising materials for EDLC construction.

On another reported work, an EDLC was prepared by using hollow microtubular benzoxazole-linked COF (TPT-DHAQ COF) as active material.[75] This hollow COF is composed of triazine core and exhibited high crystallinity, high surface area (ca. 1855 $m^2 g^{-1}$), large pore size (2.3 nm) and remarkable thermal stability. All these properties are promising for supercapacitor application. Indeed, under electrochemical analysis, the prepared cell composed of the COF exhibited rectangular shape voltammograms, even when recorded at high scan rate (200 mV s^{-1}). Meanwhile, the presence of electron-rich heteroatom species (e.g., N and O atoms) on the COF framework could stimulate Faradic storage via redox reaction. Hence, it was assumed that the capacitive response might arise from the combination of double-layers (DLs) and pseudocapacitive charge storages. Notably, a high capacitance of 256 F g^{-1} was achieved at current density of 0.5 A g^{-1}. More importantly, the cell demonstrated excellent cycling stability (98.8%) over 1850 cycles and recorded a high energy density of 43 W h kg^{-1}. Furthermore, similar capacitive behaviors were observed on the prepared capacitors composed of TPPDA-TPPyr and TPPDA-TPTPE COFs.[76] Although report on COFs for EDLC application is till rarely seen, the highly enthusiastic of researchers in designing new electroactive COFs promises great potential for developing COFs in this field.

3.1.2. Pseudocapacitors

The judicious installations of redox moieties on COFs via bottom-up and postsynthetic approaches[29,52,77] and their high thermal and chemical stability[78], make COF suitable for pseudocapacitive energy storage. Indeed, several COFs have been employed as active materials for pseudocapacitor electrodes.[32,79]

The first utilization of COFs in the field of capacitor was indeed for pseudocapacitor, reported by Dicthel and co-workers.[80] It was 2D β-ketoenamine-linked COFs (DAB-TFP COF and DAAQ-TFP COF). DAAQ-TFP COF in particular, was composed of redox-active 2,6-diaminoanthraquinone (DAAQ) moieties which can undergo reversible redox processes.

[81] In addition, it possessed high surface area (up to 1280 m^2 g^{-1}), defined eclipsed-layer structure and nanometer-scale channel (2 nm). These structural features provided an accessible high surface area and defined pathways for charge transfer to/from redox-active groups. More importantly, the presence of β- ketoenamine linkages enhanced the chemical stability of the COFs even in harsh condition (e.g., in 1 M H_2SO_4), making both COFs suitable as active materials for pseudocapacitor. Interestingly, electrode composed of 35% of DAAQ-TFP COF demonstrated a reversible Faradaic process with an *E*° of−0.058 V (*vs* Ag/AgCl) with clear oxidation-reduction peaks under cyclic voltammetry (CV) experiment in 1 M H_2SO_4 as supporting electrolyte. On the other hand, voltammogram of DAB-TFP COF (COF without redox-active DAAQ moiety) exhibited narrow voltammogram curves. This result confirmed that the Faradaic processes observed for DAAQ-TFP COF corresponded to anthraquinone reduction and oxidation reactions. Interestingly, under galvanostatic charge−discharge (GCDC) experiments, DAAQ-TFP COF could delivered capacitance as high as 48 ± 10 F g^{-1} at current density of 0.1 A g^{-1}. More importantly, significant capacitance retention (stabilized at 40 ± 9 F g^{-1}) was clearly observed even after 5000 charge−discharge cycles. This report clearly identifies the adaptability of incorporation of redox active moieties such as anthraquinone into COFs to enable them as pseudocapacitive materials. The team further explored the potential of DAAQ-TFP COF as a pseudocapacitor electrode by electropolymerizing 3,4-ethylenedioxythiophene (EDOT) monomer into the pore to achieve poly(3,4-ethylenedioxythiophene) (PEDOT)-modified DAAQ-TFP film hybrid.[82] The resultant PEDOT-modified DAAQ-TFP clearly demonstrated enhanced electrical conductivity that contributed to the dramatically improved electrochemical responses. For example, the film could tolerate high charging rate (10−1600 C) without sacrificing the charge storage performance and was able to achieve 10-fold higher current response compared to unmodified film. More importantly, the retained capacitance was even observed after 10 000 cycles.

By using the same anthraquinone building block (here as DAQ), Banerjee and team prepared ultra-highly stable, self-standing and redox active TpOMe-DAQ COF film as pseudocapacitor electrode (**Figure 3**).[40] The synthesized TpOMe-DAQ allowed for introduction of intralayer hydrogen bonding that was originated from its methoxy-functionalized building block. Hence, TpOMe-DAQ demonstrated ultrahigh chemical stability even in severe conditions (e.g., in strong acids (18 M H_2SO_4 and 12 M HCl) or bases (9 M NaOH). Interestingly, this COF film could be prepared as uniform and continuous thin sheets in centimeter scale (with the thickness of ~200 μm), thus potential for free-standing capacitor electrode. Furthermore, TpOMe-DAQ exhibited a high BET surface area (1734 m^2 g^{-1}) with 2.3 nm open pore channels. With excellent chemical stability, long-range ordered mesoporous channels and abundant redox-active groups, TpOMe-DAQ was promising as a free-standing pseudocapacitor electrode

The electrochemical analysis of TpOMe-DAQ was conducted in three-electrode system in which the COF acted as working electrode and H_2SO_4 (2 and 3 M) solution as an electrolyte. A pair of quasi-reversible redox peaks were observed under CV experiment at a lower scan rate of 1 mV s^{-1}, signifying the pseudocapacitive behavior of the COF. Impressively, the electrode showcased an areal capacitance of 1280 mF cm^{-2} (135 F g^{-1}, in 2 M H_2SO_4) and 1600 mF cm^{-2} (169 F g^{-1}, in 3 M H_2SO_4) estimated from GCD method with current density of 3.3 mA cm^{-2}. Moreover, it further demonstrated notable cyclic stability (>100,000 cycles) without obvious capacitive performance reduction. This report exemplifies that the specific design of COFs could promote the high capacitive performances which are adjustable at molecular level. The team then expanded their work through convergent synthetic method to produce series of free-standing flexible thin-sheet COF pseudocapacitor electrodes with controlled mechanical strength and redox functionality.[83] Similar pseudocapacitive performances can be expected for COFs with redox active hydroquinone (H_2Q) which can undergo reversible redox reaction into benzoquinone (Q).[84] Accordingly, two COFs with

redox-active HQ (TpPa-$(OH)_2$ and TpBD-$(OH)_2$) were prepared as active materials for pseudocapacitor electrode.[85] Particularly, TpPa-$(OH)_2$ delivered the highest specific capacitance (416 F g^{-1} at 0.5 A g^{-1}) in three-electrode system with 66% capacitance retention after 10,000 cycles at a current density of 5 A g^{-1}. More importantly, this electrode could allow for 43% accessibility of the redox-active H_2Q moieties. All these reports however, exemplify how the synthetic modulation could tune the structures and capacitive performances of COFs.

3.2. Electroactive COFs for Rechargeable Batteries

Batteries are one of the most prominent electrochemical energy storage (EES) devices due to their high energy density, high theoretical specific capacity, low-cost production, environmentally benign, and adjustable properties.[86,87] Despite tremendous efforts have been devoted in this field, the state-of-the-art battery systems are still insufficient for several aspects.[88] Particularly, conventional LIBs constructed with a graphite anode and a lithiated transition metal oxides (TMOs) cathode have reached their performance limits.[88,89] Thus, the development of advanced LIBs with high power and energy densities and long-term cycling stability is expected to emerge from new electrode materials with controlled structure-activity relationships. On the other hand, organic electrode materials have been widely explored as alternative electrode candidates for next-generation rechargeable batteries due to their distinct merits compared to the inorganic analogs.[63,90–92] For instance, they are potentially low-cost, abundant, recyclable, and safe (less exothermic) when fully discharged.

Relatively similar with pseudocapacitor, electrical energy storage in batteries involves chemical reaction (e.g., redox reaction) between intercalate ions of electrolyte and active surface of the electrode.[93] Specifically, porous organic polymers that are composed of redox active and electron-rich groups such C=O and C=N bonds are efficient for battery electrode applications, since O and N atoms could combine with metal ions (e.g., Li^+, Na^+ and K^+).[94–

[96] All these considerations point out that COFs with high chemical stability, controllable pore size and redox sites, are potential as organic electrode materials for battery application. Several reported works have indicated the utilization of COFs as active material for battery electrodes (cathode and anode), including in metal-ion batteries (Li-, Na-, K- and Zn-ion batteries), lithium-sulfur batteries (Li-S battery), and metal-gaseous battery (Li-CO_2 and Zn-air batteries).

3.2.1. Metal-ion Batteries

Development of rechargeable batteries with higher energy density, low-cost and improved safety is always highly desirable. Metal-ion batteries (e.g., Li-, Na-, K- and Zn-ion battery) are the next generation batteries that have been widely researched.[89,97–100] Interestingly, as promising organic electrode materials, COFs have also been employed in construction of such metal-ion batteries.

Lithium-ion batteries (LIBs). LIBs are widely explored due to their high voltage output and high energy density as well as low self-discharge.[89,101] On the other hand, organic materials with redox-active sites are promising candidates for LIBs because they are heavy-metal free and can be prepared from widespread resources.[87,102] Hence, as potential organic electrode, COFs with electron rich species (O, N and S) have been widely researched for LIBs electrode constructions due to the ability of those species to attract Li ions. For example, a predesigned 2D sp^2 carbon-linked crystalline conjugated polymer (2D CCP-HATN) which was contained of N-doped skeleton, was employed as high-performance LIBs cathode.[95] 2D CCP-HATN composed nitrogen-rich hexaazatrinaphthalene (HATN) derivative which was an excellent conjugated aromatic system with multiple redox-active properties.[103] More importantly, 2D CCP-HATN was crystallite into eclipsed-layer structure with a BET surface area of 317 cm^2 g^{-1} and pore sizes of 0.68 and 1.28 nm. These porosity properties could facilitate fast and efficient ions diffusion and accessible active surface. In addition, the high

chemical stability of 2D CCP-HATN could suppress the dissolution of redox-active centers. All these considerations translate 2D CCP-HATN as promising active material for LIBs cathode. Coin cell-based 2D CCP-HATN was prepared composed of Li foil acted as the counter electrode and 1.0 M LiTFSI in 1,3-dioxolane/dimethoxyethane as the electrolyte and its electrochemical behavior was investigated in a potential window of 1.2-3.9 V. For comparison, coin cell-based imine-liked 2D COF analog (2D C=N HATN) was also prepared and tested under similar condition.

The CV curve of 2D CCP-HATN exhibited four distinct redox peaks (at 1.60/1.58 and 2.45/2.4 V *vs* Li/Li^+), signaling that 2D CCP-HATN could store Li ions reversibly due to the presence of HATN as a redox-active center. Similar phenomenon was observed for 2D C=N HATN cell, although its voltammogram displayed more vague redox bands. In particular, pure 2D CCP- HATN could deliver a relatively low capacity of 62.5 mA h g^{-1} (corresponding to 53% utilization of the redox-active sites) under GCD experiment at current density of 0.1 A g^{-1}. To enhance the capacity, 2D CCP-HATN was solvothermally grown on CNTs to improve the conductivity. Hence, cell-based 2D CCP-HATN@CNT (with 50% CNT) experienced improved capacity of 116 mA h g^{-1} (approximately 73% utilization of the redox-active sites). More importantly, 91% capacity retention after 1000 cycles at 0.5 A g^{-1} and average Coulombic efficiency as high as 99.3% were observed. The work presented in this report shows the electrical capacity of battery was successfully enhanced by careful electrode design and fabrication technique, such as using COF@CTNs hybrid as active material. Furthermore, to settle more redox active sites, two imine-linked COFs (Tp–DANT-COF and Tb–DANT-COF) were prepared as potential LIBs cathode.[104] Particularly, Tp–DANT-COF was composed of N-rich naphthalene diimide and carbonyl (C=O) groups which were directly conjugated with aromatic rings. Such material composition could exhibit outstanding electrochemical performance as cathode materials for LIBs, since both groups can interact with multivalent ions.[105] As predicted, both COFs showed excellent electrochemical

performances as cathode materials for LIBs. For example, Tb–DANT-COF exhibited a high initial discharge capacity of 123.7 mA h g^{-1} (at current density 1.4 C) which was higher than Tp–DANT-COF. This distinct capacitive performance clearly identified the role of molecular structure in enhancing the electrical storage. Indeed, this report demonstrates how the chemical composition of COFs tunes the electrical capacity.

Besides by designing more redox active sites, compositing COFs with other redox-active and conductive materials (e.g., graphene, CNTs, organic polymers, and so on) are also practical to enhance the conductivity, stability and capacity of the COF-based LIBs electrode. For example, Wang and team controlled the growth of few-layer 2D imine-linked COF on CNTs to produce COF@CNTs composite as potential LIB anodes.[67] The COF (with few-layer structure) interacted with CNTs via π–π interaction and was *in-situ* separated by CNTs in the growth process (**Figure 4**). From this electrode design, the lithium-storage redox reactions can be occurred on both C=N groups and benzene rings (C=C) of the few-layered COF which means the utilization of six carbon atoms of the benzene ring to store six Li^+ ions. Furthermore, the COF possessed BET surface area as high as 44.36 m^2 g^{-1} with pore size distribution of ~1.4–1.6 nm. Meanwhile, a larger BET surface area (up to 52.73 m^2 g^{-1}) was detected for COF@CNTs composite with similar pore size distribution (~1.5 nm). Indeed, COF with a small surface area may possess short-range ordered layered structure with more defects, thus facilitate effective lithium ion diffusion. Electrochemical behavior of the prepared Swagelok-type cell composed of COF@CNTs as anode (working electrode) and lithium foil as both reference and counter electrodes was evaluated using 1 M $LiPF_6$ (dissolved in ethylene carbonate and diethyl carbonate) as supporting electrolyte.

The CV curves of COF@CNTs depicted several redox peaks attributed to the lithiation reaction with the C=N functional groups and the C=C groups of benzene rings. Impressively, COF@CNTs achieved extremely large reversible capacity of 1021 mA h g^{-1} (at 100 mA g^{-1})

after 320 cycles which can be referred to reversible capacity contribution of 1536 mA h g^{-1} from to the COF in the COF@CNTs composite. Further density functional theory (DFT) calculation revealed that lithium-ion storage mechanism in COF@CNTs was suggested to be 14-lithium-storage for a COF monomer with one Li^+ ion on per C=N group and six Li^+ ions on per benzene ring. The advantage of composing COFs with other electroactive components reported in this paper clearly showed the boosting of capacity of COF-based batteries. Indeed, compositing other COFs with CNTs has been adopted elsewhere to prepare LIBs electrodes. For example, redox-active mesoporous 2D polyimide-linked D_{TP}-A_{NDI}-COF was grown on the surface of CNTs to produce COF@CNTs composite as LIBs cathode which exhibited high efficiency, robust cycle stability, and high rate capability.[44] Nevertheless, another microporous polyimide-linked COF (PIBN) with abundant accessible carbonyl groups was *in-situ* polymerized on graphene (PIBN-G) as active material for LIBs cathode.[45] Interestingly, this COF composite achieved notable reversible specific capacities of 271 and 193.1 mA h g^{-1} at 0.1 and 10 C, respectively. In addition, it exhibited capacity retention more than 86% after 300 cycles.

Another attempt to enhance lithium capacity of COF-based LIBs electrodes was exfoliating or delaminating the COFs into few-layer nanosheets. This attempt reduces the highly layer stacking of 2D COFs which can deeply bury the redox-active sites inside the 1D channels. Hence, the resultant thin-sheets COFs enable efficient Li-ion diffusion pathway and allow for maximum utilization of redox sites inside the channels. For example, Wang and co-workers demonstrated this approach by exfoliating the prepared redox-active COF series as active materials for LIBs cathodes.[46] Based on compositions, the COFs are composed of redox actives anthraquinone (DAAQ-TFP-COF), benzoquinone (DABQ-TFP-COF), and nitroxyl radical (TEMPO-COF). Indeed, all COFs possessed similar topology. Through ball-milling method, the COFs were exfoliated to produce redox-active e-COFs. The resultant e-COFs structurally mimicked graphene with the addition of adjustable atomic structures and

ordered channels. Interestingly, all resultant e-COFs showed retained major PXRD patterns, indicating the preservation of the structural order. However, all e-COFs demonstrated surface area reduction as consequence of layer delamination. In addition, they still manage several layers (10-15 layers), yet were much thinner than their pristine COFs. This structural fashion could ensure efficient and rapid Li^+ ion storage. Indeed, under CV experiment, the prepared battery cells composed of e-COFs as cathode and metal lithium as anode exhibited clear redox peaks which mean reversible lithiation/delithiation reactions took place. Meanwhile, GCD analysis revealed that DAAQ-ECOF delivered high reversible capacity of over 145 and 107 mA h g^{-1} at 20 and 500 mA g^{-1}, respectively, while maintaining 98% of its capacity after 1800 deep discharge-charge cycles. Furthermore, it showed doubled (at 500 mA g^{-1}) and even tripled (at 3000 mA g^{-1}) capacities compared to its un-exfoliated pristine COF. Indeed, similar phenomenon was also observed for other two e-COF cells with higher theoretical capacity and voltage plateaus. For example, DABQ-ECOF and TEMPO-ECOF exhibited 35 and 53% capacities higher than their pristine COFs at 20 mA g^{-1}, respectively. Particularly, DABQ-ECOF achieved specific capacity of 210 mA h g^{-1} and a voltage plateau of 2.8 V. Similarly, Huang and team also demonstrated this approach by preparing a few-layer polyimide-COF (PI-ECOF) and further composite it with reduced graphene oxide (PI-ECOF/rGO composite) as cathodes for LIBs.[106]

Sodium-ion Batteries (SIBs). SIBs have been regarded as attractive alternative electrochemical devices because sodium (Na) is of naturally abundance, low-cost, and environmentally friendliness and they have a comparable theoretical energy density with LIBs.[97,107] On the other hand, organic electrodes can offer a potential opportunity to achieve high migration kinetics of Na^+ ions due to their structural flexibility.[98] Hence, COFs as potential organic electrodes hold great prospects for SIBs.

Chen and team prepared a honeycomb-like N-rich 2D COF (TQBQ-COF) with multiple carbonyls as active material for SIBs cathode.[49] TQBQ-COF was composed of triquinoxalinylene and benzoquinone units which was obtained from condensation reaction between tetraminophenone (TABQ) and cyclohexanehexaone (CHHO). Structurally, TQBQ-COF possessed dual redox-active pyrazine (C=N) and carbonyl (C=O) groups in its skeleton which could become the active sites for Na^+ ions storage. According to in/ex-situ Fourier transform infrared (FTIR) spectra and DFT calculations, twelve Na^+ ions (including six Na^+ ions within the TQBQ-COF plane and another six Na^+ ions outside the plane) could be stored per TQBQ-COF repetitive unit. On the other hand, TQBQ-COF was crystalline material with BET surface area of 94.36 $m^2\ g^{-1}$ and hexagonal micropores size of 1.18 nm (after activated at 200 ˚C for 5 h). This moderate surface area was reasonable, since TQBQ-COF was obtained as thin-layer COF (according to TEM and AFM analyses). The sodium storage capacity of TQBQ-COF was analyzed by preparing battery cell composed of TQBQ-COF as cathode and sodium disk as the counter electrode.

The CV curves of TQBQ-COF displayed obvious two couple redox peaks corresponding to the successive two-step sodiation/desodiation process. Meanwhile, under GCD experiment, TQBQ-COF could deliver an initial discharge capacity of 452.0 mA h g^{-1} (at 0.02 A g^{-1}, 1~3.6 V). Notably, a high specific capacity of ~400 mA h g^{-1} was obtained after 10 cycles and as high as 352.3 mA h g^{-1} can be maintained even after 100 cycles at similar current density (0.02 A g^{-1}). More importantly, this electrode could exhibit excellent rate capability and cycling stability, such as capacity retention of 96.4% were achieved even after 1000 cycles at 1.0 A g^{-1}. Meanwhile, SIBs anode was constructed by using a mesoporous 2D imine-linked COF (TFPB-TAPT).[108] TFPB-TAPT was composed of electron-rich triazine units and imine linkages which can be redox-active sites for sodium storage. Indeed, SIBs cell composed of TFPB-TAPT as anode displayed clear anodic and cathodic peaks under CV analysis (at 0.02 mV s^{-1}, 0.001–3.0 V), implying the reversible Na^+/Na redox system. Notably, the electrode

could deliver an initial reversible capacity of 246 mA h g^{-1} for the 2th cycle at 30 mA g^{-1}. Meanwhile a high capacity of 125 mA h g^{-1} can be reached even after 500 cycles at similar current rate. These two reports exemplify the tunable sodium capacity of COFs via composition tuning and structural modulations.

Zinc-ion batteries (ZIBs) and Potassium-ion Batteries (PIBs). Similar with SIBs, both ZIBs and PIBs are promising next-generation electrochemical energy storage devices. Both kinds of batteries are plausible alternatives to LIBs because these devices are based on relatively abundant and low-cost elements (Zn and K) and they have similar chemical properties to lithium.[100,109] Rechargeable batteries with multivalent carrier (such as Zn^{2+}) can, in principle, achieve higher specific capacity and energy density due to the multiple electrons involved in redox reactions, and superior in terms of safety and recyclability than the monovalent LIBs and SIBs.[110,111] Nevertheless, since K in particular, could offers a lower reduction potential (relative to Na), KIBs enable to operate at higher potentials to improves energy density.[99] Hence, both types of battery hold great future for development of batteries.

COFs have also been explored as active materials for both ZIBs and PIBs electrodes construction recently, due to their structural designability, high chemical and thermal stabilities, and tailorable functionalities. However, since both Zn^{2+} and K^{+} ions have bigger kinetic-diameter size than Li^{+} ion, specific design of COFs with sufficient porosity is pivotal to allow those ions to travel within the electrode. For example, Banerjee and team designed hydroquinone based β-ketoenamine linked COF (HqTp) that is able to host Zn^{2+} ions as cathode material for rechargeable ZIBs.[58] Since C=O and N–H functionalities in polymers are capable in coordinating Zn^{2+} ions in an electrochemical cell[59,112], electron-rich carbonyl and enamine groups on HqTp could coordinatively engage Zn^{2+} ions. Furthermore, HqTp was highly crystalline material with BET surface area of 113 $m^2 g^{-1}$ and a pore size of 1.5 nm. An aqueous ZIBs cell was prepared using HqTp as cathode material and Zn foil as anode. CV

curves of the prepared cell exhibited distinct pair redox peaks (at 0.1 mV sec^{-1}), indicating the quinone oxidation-reduction reaction occurred. Meanwhile, GCD experiment revealed a notable discharge capacity as high as 276 mA h g^{-1} (at 125 mA g^{-1}) was achieved by the cell. This capacitive achievement might arise from the efficient reversible interlayer interaction of Zn^{2+} ions with the functional groups in the COF.

As for PIBs, COFs should possess sufficiently large pore size, since the large radius (1.38 Å) of K^+ ions could severely hinder the ions insertion into the electrode material and therefore resulted in low electrochemical activity. In the following report, few-layer mesoporous boronate ester-linked COF (COF-10) deposited on the exterior surface CNTs (COF-10@CNT) and further used as anode material for rechargeable PIBs.[113] Both COF and CNTs interacted via π−π stacking interaction. Meanwhile, it has been found that metal cations such as Li^+, Na^+, K^+, Mg^{2+} and Ca^{2+} could build strong cation−π interactions with 2D carbon materials.[114,115] Hence, COF-10 which rich of π−conjugated aromatic benzene rings could facilitate strong interaction towards for K^+ ions. COF-10 exhibited strong PXRD peaks, indicating its high crystallinity. Interestingly, those PXRD peaks were still observed in COF-10@CNT. COF-10@CNT in particular, possessed pore size of ~3.09 nm which was large enough to allow K ions to travel. Interestingly, COF-10 was found as thin-layer (~ 6 nm) uniformly covered the exterior surface of CNTs. Hence, presence of hierarchical pores within the few-layer COF in the COF-10@CNT shorten the ion/electron diffusion distance and enhance the insertion/extraction kinetics of K^+ ions.

Electrochemical behavior of COF-10@CNT was analyzed by preparing anode for PIBs. The CV curves of COF-10@CNT clearly depicted a cathodic (at 0.61 V) and three anodic peaks (at 0.81, 0.54, and 0.31 V), corresponding to potassisation and depotassisation processes, respectively. Meanwhile, it manifested an initial charge capacity of 348 mA h g^{-1} (at 100 mA g^{-1}) which was larger than COF-10 (130 mA h g^{-1}). Notably, COF-10@CNT

could preserved high capacity of 288 mA h g^{-1} even after 500 cycles (at 0.1 A g^{-1}) which was much larger than COF-10 (57 mA h g^{-1}). Furthermore, it still preserved sufficient capacity (161 mA h g^{-1}) even after deep-cycles (4000 cycles at 1 A g^{-1}), signaling the high-rate cycling performance. Indeed, this report could provide insights in designing other COFs as active materials for PIB electrodes.

Lithium-Sulfur Batteries (LSBs). In the virtue of high energy density, lithium-sulfur batteries (LSBs) are the most promising next-generation high energy density rechargeable batteries to replace LIBs due to their high energy density (2600 Wh kg^{-1}) and exceptional theoretical capacity (1672 mA h g^{-1}).[116,117] However, unlike with the other previous metal-ion batteries, LSBs produce high-order lithium polysulfides (PSs) (Li_2S_x, $4 \leq x \leq 8$) as intermediate redox species during charge-discharge processes which caused "*shuttle effects*" phenomenon.[118] This drawback will lead to the limitation of capacity in the sulfur electrodes (much below than their theoretical value), an infinite recharge, big active mass loss, and poor cycle life.[119,120] Thus, specific design of electrodes that can reduce this shuttle effect is pivotal to improve the capacity performances of LSBs. As promising organic electrodes, COFs with their high surface areas, tunable functional modulation, and high chemical and thermal stabilities, are potential hosts to store sulfur and fully confine the mobile redox PS species. All these considerations, render COFs as potential porous materials for LSBs.

Tang and co-workers utilized boroxine-linked COF (COF-1) that was able to chemisorb sulfur and trap PS species as LSB cathode material.[68] Since COF-1 was composed of positively polarized B and negatively polarized O, it can sufficiently absorb sulfur molecules via simple thermal impregnation (to produce COF-1/S).[119,121] COF-1 was high crystalline and microporous material. Upon compositing with S, the PXRD peaks were ultimately disappeared indicating the highly dispersion of sulfur (40%, evidenced by TGA analysis) on the matrix of COF-1. This LSB cathode design will guarantee the efficient adsorption of Li^+

ions and trapping of LiPSs within the cathodes, thus enhanced capacity storage. The lithium capacity of COF-1/S in LSBs was explored by preparing coin-type cell composed of COF-1/S as cathode and Li metal as anode. The CV curves of the cell discerned well-defined two reduction peaks, corresponding to reduction reactions of elemental sulfur to LiPSs and to Li_2S_2/Li_2S, respectively, while another two overlapped oxidation peaks were also observed belonging to the stage transition of Li_2S to PSs species to elemental sulfur. Meanwhile, electrochemical impedance spectroscopy (EIS) measurements showed the dropping of resistance from 85 to ≈57 Ω after 60th and 100th cycles, proving the effective LiPSs species trapping within the electrode and reduction of insulating layer formation on the cathode surface. Notably, the cell could deliver an initial specific capacity of 1628 mA h g^{-1} (at 0.2 C), and retained it up to of 929 mA h g^{-1} after 100 cycles. In addition, this battery exhibited remarkable cycling stabilities at different current densities. Impressively, a reversible capacity of 1048 mA h g^{-1} was successfully retained once the current was set-back from 1 to 0.1 C. This remarkable capacity rose from the well-defined pores and abundant sulfur elements in COF-1/S cathode. Furthermore, by using CTF-1 instead of COF-1, CTF-1/S @155˚C was prepared as cathode material for LSBs.[122] Nevertheless, besides by thermal impregnation, concentrating sulfur into COFs to translate them as potential LSBs cathode, can also be performed by covalently linking sulfur units onto the highly fluoro-functionalized COF (COF-F to COF-F-S).[41]

On another occasion, by using boroxine and boronate ester-linked COFs with different pore sizes, self-standing COF-1(0.7 nm) and COF-5 (2.7 nm) was deposited on mesoporous CNT net and were explored as an alternative PS trap es for LSBs.[123] The distinct pore size of both COFs could provide an interesting study on how the pore size influenced Li_2S_x species trapping in LSBs. Specifically, these COF-net on CNT-net (called “NN interlayers”) hybrids were prepared by CNT-templated *in-situ* COF synthesis. The resultant NN hybrids have flexible paper-like structure with average thickness of ~45 μm. In addition, with COF-5

(COF-5 NN), a more uniform/homogeneous surface morphology was observed compared to COF-1 NN. Indeed, this electrode architecture was expected to allow for facile ion transport (through mesopores) and the effective LiPSs species trapping (predominantly by micropores) without impairing its electronic conduction. Under electrochemical analysis, the CV profiles of both hybrids exhibited overlapped oxidation peaks and two separated reduction peaks corresponding to charge/discharge process of soluble long-chain Li_2S_x to insoluble low-order Li_2S_2/Li_2S and oxidation of Li_2S/Li_2S to Li_2S_8/S. Further electrochemical measurement revealed that the COF-1 NN demonstrated a significantly improved capacity retention (84%) after 300 cycles at current density of 2.0 C/2.0 C compared other prepared cells (below 16%). Meanwhile, the distinct capacity retentions (at the lower current density of 0.2 C) might due to the different PSs capture ability of COF hybrids and time for the deposition/dissolution of insoluble lithium PSs in interlayers. Furthermore, besides as active material for electrodes, electroactive COF (e.g., Tp-BPY-COF) has also been employed as separator in LSBs cell.[124] The well-defined of 1D pore channels and the presence of electroactive pyridine units in Tp-BPY-COF, allowed for a fast transport of the Li^+ ions, enhanced sulfur adsorption and boosted the charge/discharge processes. Nevertheless, the reports discussed in this sub-section clearly show the great potential of COFs for LSBs application, not only as electrode materials but also potential for battery spare-parts (e.g., separator).

3.2.2. Metal-Air Batteries

The effort toward designing greener and safer rechargeable batteries has arrived at the utilization of air (O_2 and CO_2 gaseous) as part of the electrodes (e.g., cathode), which are naturally abundance, non-toxic, economic, and environmentally benign.[125–127] The rechargeable nonaqueous metal–air batteries have attracted considerable attention as future electrical storage devices due to their high theoretical energy density (e.g., 3500 Wh kg^{-1} for Li–O_2 batteries or 1600 Wh kg^{-1} for Na–O_2 batteries).[128–130] In consideration with COFs as

promising organic electrode materials, their ordered porosity, tailorable structures and chemical functionalities that are able to attract gaseous (e.g., CO_2), and high chemical and thermal stabilities[24,78], hold great opportunity as electrode material for metal-air batteries. Although, the research of nonaqueous metal-air batteries is still infancy compared to LIBs and SIBs, electroactive COFs have also been utilized as electrode materials for this type of battery.

Practically, due to their ability to capture gas (such as CO_2), COFs can potentially act either as solely electrode or as CO_2 collector when combined with the main electrode active material. For example, Loh and team designed hydrazone-linked COF (Tf–DHzOPr COF) and then hybridized it with Ru@CNT (COF-Ru@CNT) as cathode in Li-CO_2 batteries.[131] In this electrode design, the channel of COF which acted as CO_2 collector and diffusion channels for both ion and gas (once interfaced to Ru@CNT), while Ru was a catalyst that was responsible for both CO_2 reduction and Li_2CO_3/C decomposition.[132] The presence of ketone and imine functional groups in the COF facilitate coordination bond with Ru, thus the edges of COF were interfaced with Ru@CNT. This hybrid fashion gave rise to shorter paths to catalytic sites for CO_2 molecules and Li^+ ions. The COF was crystalline with BET surface area of 871 $m^2\ g^{-1}$ and pore size of 1.69 nm. Meanwhile, COF-Ru@CNT possessed BET surface area of 354 $m^2\ g^{-1}$ with similar pore size. Interestingly, COF-Ru@CNT could exhibit CO_2 uptake as high as 23.2 $cm^3\ g^{-1}$ (1 atm, 273 K) and 13.4 $cm^3\ g^{-1}$ (1 atm, 298 K), respectively. This notable CO_2 capacity along with the well-defined channel in COF-Ru@CNT promise application in Li-CO_2 batteries. Accordingly, Li-CO_2 batteries cell was prepared which composed of COF-Ru@CNT as cathode and Li metal as anode. The cell based on CNT, Ru@CNT and COF-CNT were also prepared for comparison. Remarkably, COF-Ru@CNT exhibited ultrahigh capacity of 27,348 mA h g^{-1}, extremely higher than CNT (9045 mA h g^{-1}), Ru@CNT (9836 mA h g^{-1}) and comparable with COF-CNT (25,163 mA h g^{-1}) at current density of 200 mA g^{-1}. These results confirmed that the presence of COFs enhanced the capacity of the cell due to its ability to boasts the CO_2 intake of the electrode, while its high

surface area provided space for formation of discharge products (Li_2CO_3/C). More importantly, the battery could run for 200 cycles even at high current density. Indeed, this report clearly indicates the potential of COFs for metal-air batteries under specific design electrode.

3.3. Electroactive COFs for Conductors

Conductive materials are widely used in electronics and electrochemical energy conversion and storage devices (such as capacitors, batteries, and fuel-cells).[133] Conductivity property allows for efficient transport and mobility of charges and ions in porous materials. Practically, based on their mechanism and applications, conductive materials are classified as electrical and ionic conductors. As tailorable porous materials, MOFs have been widely designed and explored as promising conductive materials.[134] In general, like MOFs, COFs are less-conductive porous materials.[134,135] However, under specific structural design, such as introduction of electroactive building units, settlement of electroactive functionalities and compositing them with conductive components, COFs can be transformed into high conductive materials.[78] Ideally, 2D COFs which are generally rich of π-conjugated system and shorter layer-to-layer distances could stimulate electronic interactions between their layers, and hence potentially become a conductive materials.[136] Meanwhile, 3D COFs which generally possess high surface areas could load more conductive components, thus enhanced the conductivity. In this sub-section, the design of electroactive COFs and their applications for electrical and ionic conductivities are elaborated.

3.3.1. Electrically Conductive COFs

Their periodical structure, extended conjugation, permanent porosity, and tunable compositions and functionalities, make COFs emerging as promising kind of electroactive organic materials that are able to demonstrate electrical conductivity.[32] As previously demonstrated in MOFs, chemical doping strategy could enhance the electrical conductivity of

the compounds up to six orders of magnitude higher.[137] Thus, preparing COFs by doping with electron/charge donor-acceptor constituents could, in principle, enhance their electrical conductivity.

For example, an oriented thin film COF (TTF-COF) composed of tetrathiafulvalene (TTF) units was developed and explored for electrical conductivity.[138] The thin film was then doped with I_2 or tetracyanoquinodimethane (TCNQ) dopants (TTF-COF/I_2; TTF-COF/TCNQ). As widely known, TTF is an excellent electron donor that is able to form highly conductive charge-transfer crystals with electron acceptors such as I_2 or TCNQ[139,140], while the well-defined framework of the thin film with stacked TTF columns could provide conductive pathways. Hence, both TTF-COF/I_2 and TTF-COF/TCNQ films could provide stage for the generation of mixed-valence TTF stacks, which was essential for high conductivity. The films were crystalline having preferential orientation of the columns normal to the substrate support and possessed nominal thickness of around 150 nm. The conductivity of both doped films was tested and their current-voltage (*I*-*V*) curves were analyzed. With pristine TTF-COF film, a linear *I*-*V* curve was obtained corresponding to a moderate conductivity of 1.2×10^{-4} S m^{-1}. Notably, significant conductivity improvements were seen upon doping with I_2 or TCNQ. For example, conductivities as high as 0.28 S m^{-1} was documented once the film was exposed with I_2 (TTF-COF/I_2) in chamber for 24 h. Meanwhile, after removing from chamber and left in air for 48 h, the film still managed a conductivity of 1.0×10^{-3} S m^{-1}. Similar phenomenon was also shown by TTF-COF/TCNQ sample, indicating the effectiveness of chemical doping to increase the conductivity of pristine COF. Electron paramagnetic resonance (EPR) analysis was then administered to further study the doping effect. EPR spectrums of TTF-COF film displayed a weak signal, indicating the presence of very small amount of paramagnetic $TTF^{\bullet+}$. Meanwhile, notable paramagnetic intensities enhancements were observed for both TTF-COF/I_2 and TTF-COF/TCNQ samples, clearly

clarifying the increased $TTF^{\bullet+}$ concentration in-line with doping degree. Furthermore, by slightly varying the pore size of the COFs, other I_2-doped TTF-based COF analogs were also reported elsewhere for similar electrical conductivity application.[141,142]

Inspired by the previous report mentioned above, Fang and team developed high surface areas, high crystalline and electroactive 3D COFs composed of TTF units (3D-TTF-COFs; JUC-518 and JUC-519) and explored them for electrical conductivity.[35] JUC-518 was obtained by condensing TTF derivative of tetrathiafulvalene-tetrabenzaldehyde (TTF-TBA) with 4-connected 1,3,5,7-tetraaminoadamantane (TAA) (**Figure 5**). Meanwhile, by using tetra(4-aminophenyl)methane (TAPM) instead of TAA, JUC-519 was judiciously obtained. Interestingly, both 3D COFs possessed **pts** topology as predicted, in which JUC-518 had non-interpenetrated structure, while for JUC-519 was 2-fold interpenetrated structure. JUC-518 showed notable high BET surface area (3018 $m^2 g^{-1}$) which was almost doubled than JUC-519 (1513 $m^2 g^{-1}$). Meanwhile, they exhibited a pore size of 1.54 and 0.84 nm for JUC-518 and JUC-519, respectively. Both COFs were then doped with electron acceptor I_2 molecules. Practically, the 3D COFs were exposed with I_2 vapor in which oxidation of TTF could happened in this stage, since I_2 can act as suitable oxidant.[143] Obviously, the EPR spectrum of pristine 3D COFs displayed very weak signals, while significant paramagnetic intensities increasement (by approximately 2 orders of magnitude higher) after doping treatment was clearly observed, confirming the enhancement of $TTF^{\bullet+}$ concentration.[144] Interestingly, the PXRD pattern of both 3D COFs were retained even after 48h doping, signaling their structural integrities. Having these results, the electrical conductivities of the I_2 doped 3D-COFs were then evaluated through two-probe configuration. Interestingly, the electrical conductivities of the samples were varied depending on the doping time and temperature setting. For example, JUC-518 exhibited electrical conductivity of 2.9×10^{-7} S cm^{-1} at 25 ^{o}C after doping for 6 h, which was increased to 2.7×10^{-4} S cm^{-1} after 48 h and extremely escalated to 1.4×10^{-2} S cm^{-1} once the temperature was raised to 120 °C. Comparatively, these electrical conductivity

performances were superior than previously reported 2D-TTF-COF powder (~10^{-5} S cm^{-1})[141,142] and comparable with several TTF-based MOFs (~10^{-4} S cm^{-1}).[145–147] Furthermore, similar phenomena were also seen for JUC-519, although its conductivities was relatively lower than JUC-518. Indeed, this report clearly demonstrated the tuning of electrical conductivity of COFs through compositions and porosity tailoring, which can promote wider applications of COFs in molecular electronics and energy storages.

Jiang and team, on another occasion, reported the impressive electrical conductivity enhancement of the of the pristine COF upon I_2 doping.[148] The COF (sp^2c-COF) was 2D fully π-conjugated structure and constructed from all sp^2 (C=C) carbons. Structurally, sp^2c-COF composed of π conjugation along both the x and y directions that can offer sp^2 carbon lattice structure. In addition, this COF exhibited high BET surface area of 692 m^2 g^{-1} and micropore size of 1.88 nm. To further explore the electrical conductivity of sp^2c-COF, it was then oxidized (doped) with I_2. The EPR spectroscopy measurement confirmed the increasement of peak-to-peak height of *g*-factor (at 2.003) during 3 mins to 1 day after doping. This EPR signal increasement indicated the generation of charge carriers which possess a spin degree of freedom. Interestingly, I_2-doped sp^2c-COF demonstrated linear *I-V* curve, an indicative of ohmic conductivity. From this curve, the electrical conductivity was determined. Impressively, the electrical conductivity was obtained as high as 7.1×10^{-2} S cm^{-1} which was 12 orders of magnitude higher than pristine sp^2c-COF (6.1×10^{-14} S cm^{-1}). Indeed, the electrical conductivity of I_2-doped sp^2c-COF was much higher than previously reported 2D/3D TTF-COFs discussed above.[35,138,141,142] On the other hand, beside doped with electron acceptor I_2, polymerizing conductive polymer into the pore of electroactive COFs, has also been reported to enhance the electrical conductivity of COFs.[149] All reports presented in this sub-section show the robust and tunability of COFs in structural and compositional modifications to enhance their electrical conductivity.

3.3.2. Ionic Conductive COFs

Ionic conduction plays pivotal role in energy storage and conversion devices.[150] Ionic conductive materials are important and highly demanded in fuel-cells and electronics due to their ability to transport ions (H^+, Li^+, Na^+ and Mg^{2+}) at the certain medium or porous surface.[134] In particular, the research of proton (H^+) and lithium (Li^+) conducting materials have sparked tremendous interest for their widely employment in fuel-cells and batteries.[151,152] COFs with their tailorable porosities and functionalities[25,53,78] are perfect materials for proton and lithium conductions.

Proton Conduction. Proton conducting materials have widely been researched for their applications in fuel-cells, sensors, and electronic devices.[153] Materials for proton conductor are always referred to Nafion-based proton conducting membrane as benchmark that exhibited high proton conductivity (~10^{-1} S cm^{-1} at 60−80 °C, 98% relative humidity (RH)).[153] In their developments, several organic porous materials and even MOFs have been designed and explored for proton conduction application.[154–157] Hence, COFs with flexible incorporation of wider functionalities, and high chemical and thermal stabilities could, in principle, be perfect porous materials for proton conduction.[25,28,78,158] Typically, proton conduction was conducted at humid condition, thus hydrolytical stablities are pivotal for this application. Meanwhile, to allow the protons to travel, porous materials should provide active sites, proton sources or even carrier to support the conductivity.[159,160]

Zhao and team, bottom-up synthesized sulfonated COF (NUS-10) which was rich of sulfonic acid pendant groups as proton conductor material.[54] Although this COF was less-crystalline and possessed low BET surface area (only 69 m^2 g^{-1}), the presence of sulfonic acid groups in the 1D channels, may beneficial for proton conduction. Indeed, under proton conduction experiment, NUS-10 could intrinsically conduct proton as high as 3.96×10^{-2} S cm^{-1} and this performance was stable for long-term at ambient temperature and high humidity

(97% RH). Besides with functional groups, doping with proton source could also transform COFs into proton conducting materials. For example, Banerjee and team designed chemically stable 2D COF (Tp-Azo) that can be doped with phosphoric acid (PA, H_3PO_4) for proton conduction.[47] Tp-Azo was crystalline material and possessed keto-enamine form which lead it to be stable toward boiling water, strong acidic, and basic media. More importantly, the presence of azo (-N=N-) moieties can stabilize H_3PO_4 molecules once protonated, while $H_2PO_4^-$ anions would be stabilized by H-bonds[48]. Hence, Tp-Azo was undoubtedly a perfect material for proton conduction. Subsequently, Tp-Azo was loaded with H_3PO_4 to produce PA@Tp-Azo. For comparison, another 2D COF analog (Tp-Stb, without azo moiety) was also loaded with H_3PO_4 (PA@Tp-Stb). All PA@COFs were further tested for proton conduction. Interestingly, PA@Tp-Azo demonstrated high proton conductivities of 9.9×10^{-4} S cm^{-1} at 332 K (98% RH) and 6.7×10^{-5} S cm^{-1} at 340 K (anhydrous). In contrast, PA@Tp-Stb was proton insulator at anhydrous condition and only conducted proton as high as 2.3×10^{-5} S cm^{-1} at 332 K under 98% RH. This report shows the proton conductivity of COFs can be adjusted via composition tuning.

Polyoxometalates (POMs) are nanosized clusters that have been widely explored for catalysis, electronic devices and fuel-cell.[161,162] POMs have also been loaded into COFs to enhance the proton conductivity of COFs. For example, a cationic 2D COF that are composed of exchangeable Br^- counterions (EB-COF:Br) was designed as host to accommodate POM ions (PW_{12}; $PW_{12}O_{40}^{3-}$) for proton conduction.[163] The EB-COF:Br was bottom-up synthesized by using a cationic building block of ethidium bromide (EB) and 1,3,5-triformylphloroglucinol (TFP). Interestingly, the resultant EB-COF:Br was crystalline, chemically stable (even in 3 M HCl for 7 days) and possessed high BET surface area of 774 m^2 g^{-1} and a pore size of 1.66 nm. Upon anion exchange with PW_{12} ions (having ionic size of around 1.2 nm), the resultant EB-COF: PW_{12} experienced drastically surface area reduction (down to 8 m^2 g^{-1}). EB-COF: PW_{12} was then explored for proton conduction under controlled

RH. For comparison, the proton conductivity of EB-COF:Br was also analyzed. Interestingly, the proton conductivity of EB-COF: PW_{12} reached as high as 3.32×10^{-3} S cm^{-1} at 25 °C (97% RH), which was almost 100 times higher than EB-COF:Br (2.82×10^{-6} S cm^{-1}) at similar condition. It was assumed that the presence of PW_{12} molecules within the channel, could attract water molecules around them, hence enhanced proton conductivity. This result, clearly shows the contribution of POMs in enhancing the proton conductivity of COFs.

An impressive design of COFs for proton conductivity was reported by Jiang and team. The team loaded *N*-heterocyclic proton carriers (triazole (trz) and imidazole (imi)) into the channel of highly stable and mesoporous 2D TPB-DMTP-COF as proton conductor materials.[164] The COF host was very crystalline and exhibited high BET surface area of 2,072 m^2 g^{-1} with large pore size (3.26 nm) and high pore volume (1.34 cm^3 g^{-1}). In addition, this COF was chemically stable in water (at 25 and 100 °C), in strong acid (12 M HCl, 25 °C) and strong base (14 M NaOH, 25 °C) for one week and was thermally stable (up to 400 °C in N_2 and 340 °C in oxygen). The high pore volume and remarkable stabilities allowed for efficient thermal loading of trz and imi molecules to obtain two composites of trz@TPB-DMTP-COF and im@TPB-DMTP-COF, respectively. Severe surface areas reduction was clearly observed in both materials, such as down to 0.4 m^2 g^{-1} in trz@TPB-DMTP-COF (corresponding to 180 wt% of trz loaded) and 2.3 m^2 g^{-1} in im@TPB-DMTP-COF (corresponding 155 wt% of imi loaded), respectively. Having high proton carrier loaded in both materials, the proton conductivity was then performed under varied temperatures. Impressively, trz@TPB-DMTP-COF conducted proton as high as 7.0×10^{-4} and 1.1×10^{-3} S cm^{-1} at 100 and 130 °C, respectively. Indeed these performances were superior than the state-of-the-art triazole-loaded MOFs composed of microporous sulfonated β-PCMOF2 (3×10^{-4} S cm^{-1} at 130 °C).[160] Meanwhile, imi@TPB-DMTP-COF also exhibited notable proton conductivity of 1.79×10^{-3} and 4.37×10^{-3} S cm^{-1} at 100 and 130 °C, respectively. Interestingly, imi@TPB-DMTP-COF experienced negligible conductivity reduction under a

24 h continuous run at 130 °C. Meanwhile, on another occasion, Banerjee and co-workers, prepared self-standing and flexible COF membranes (COFMs) as superprotonic conductor materials.[165] The COFMs were prepared by loading *p*-toluene sulfonic acid (PTSA.H_2O) during COFs synthesis to produce PTSA@COFMs series (PTSA@TpBpy, PTSA@TpAzo, and PTSA@TpBD$(Me)_2$). All membrane showed significantly superior proton conductivities, in which PTSA@TpAzo exhibited the highest proton conducting ability (6.3×10^{-2} and 7.8×10^{-2} S cm^{-1} at 30 and 80 °C under 95% RH, respectively). Indeed, this report could inspire the fabrication of COF membrane-based proton conductor for fuel-cell application.

Lithium Conduction. Among numerous next-generation battery systems explored to date, metal-ion batteries such as LIBs and SIBs have been widely explored.[89,97] Such a great interest toward these batteries procures the lithium and sodium conductors as the key materials for development of LIBs and SIBs. Particularly, in lithium conducting materials, conductivity is related to the product of the Li^+ ions concentration and mobility.[166] Thus, to design lithium conductor, the materials should be able to concentrate Li^+ ions and allow them to efficiently mobile. As highly porous material with tailorable active sites for engaging ions and high thermal and chemical stabilities,[25,28,53,78] COFs can, in principle, accommodate lithium salts and thus potential for solid-sate lithium conductor. Indeed, several reports have indicated the exploration of COFs for lithium conduction.

Typical design of COFs for lithium conductor was COFs with ionic structures that are able to concentrate Li^+ ions. In delight, a spiroborate-linked COF (e.g., ICOF-2) which possessed immobilized sp^3 hybridized boron anionic centers linkages was prepared as solid-state lithium conductor.[50] More importantly, the linkages (spiroborates) of ICOF-2 have been found to be chemically stable, including in water, methanol, and under basic conditions.[167] Structurally, the anionic spiroborate linkages of ICOF-2 were stabilized by mobile Li^+ ions, hence potential for solid-state lithium conduction. The prepared ICOF-2 film

was then tested for lithium conduction. Remarkably, ICOF-2 exhibited room-temperature lithium conductivity as high as 3.05×10^{-5} S cm^{-1}. In addition, it delivered an average Li^+ transference number (t_{Li^+}) of 0.80±0.02 which was significantly higher than those typical solid-state polymer electrolytes with dopant lithium salt (t_{Li^+} = 0.2–0.5).[167] Inspired by this report, 3D spiroborate-linked cyclodextrin COF (e.g., CD-COF-Li) was designed for similar application.[168] Interestingly, after immersing in $LiPF_6$ in (ethylene carbonate (EC) and dimethyl carbonate (DMC)), CD-COF-Li (denoted as CD-COF-Li⊃$LiPF_6$-EC-DMC) was lithium conductible with impressive lithium conductivity up to 2.7×10^{-3} S cm^{-1} (at 30 °C). This remarkable conductivity was assumed due to the flexible and dynamic nature of CD moieties, the abundance anionic spiroborate linkages, and the high capability for entrapping the electrolytes in the confined channels.

Beside with anionic skeleton, COFs with cationic skeleton can also act as solid-state lithium conductor. For instance, a predesigned cationic COF nanosheet (CON-Cl) was a typical solid-state lithium conductor which was composed of cationic N^+ skeletons stabilized by Cl^- ions.[51] These cationic moieties could split the ion pair of Li salt, hence able to drastically concentrate mobile Li^+ ions for lithium conductivity. Experimentally, CON-Cl was ion-exchanged with lithium bis(trifluoromethane)sulfonimide (LiTFSI), in which Cl^- ions were replaced with $TFSI^-$ ions (CON-TFSI). Finally, it was mixed with LiTFSI salt to concentrate mobile Li^+ ions within the cationic channel (Li-CON-TFSI). Li-CON-TFSI exhibited PXRD peaks disappearance relative to CON-Cl as consequence of LiTFSI salt deposition. In addition, Li-CON-TFSI was a loose and irregular 2D nanosheet with average thickness of 5 nm and exhibited BET surface area of ~118 m^2 g^{-1}. Under conductivity experiment, Li-CON-TFSI exhibited lithium conductivity as high as 5.74×10^{-5} and 2.09×10^{-4} S cm^{-1} at 30 and 70 °C, respectively and had a t_{Li^+} value of 0.61 ± 0.02. Interestingly, unlike in the previous 2D/3D ICOFs mentioned above[50,168], Li-CON-TFSI was solvent-free

lithium conductor, thus demonstrating safety aspect (reduced possible flammability). Based on the structural evolution study, it was assumed that Coulombic interaction between cationic framework and the ion species (including free Li^+ cations, free $TFSI^-$ anions, and the ion pairs of Li^+−$TFSI^-$) may occur, in which the cationic framework electrostatically interacted with $TFSI^-$ anions and liberated Li^+ ions for faster ion conduction. Nevertheless, this work could inspire the design of cationic COFs that are potential for conducting other ions such as Na^+, K^+, Mg^{2+}, or Al^{3+} in the future reports.

On the other hand, installing ionic pendant groups in COFs could act as immobilized active centers for concentrating Li^+ ions, thus enhancing lithium conductivity. Indeed, several COFs with ionic and electron-rich pendant groups have been designed for lithium conductor. For example, Zhang and team designed a series of imidazolate-containing ionic COFs (R-ImCOFs; R= H, CH_3 or CF_3) as single-ion solid-state lithium conducting COF (**Figure 6**).[169] R-ImCOFs are composed of imidazolate anions that can form loose bonding with Li^+ ions as demonstrated in lithium-imidazolate salt.[170] Hence, R-ImCOFs were structurally able to concentrate Li^+ ions, in which imidazolate anions were immobilized as pendant groups, leading to the single-ion (Li^+) conductor. Such kind of conduction could enhance ions transference number and avoid undesired side reactions. R-ImCOFs were highly crystalline materials and exhibited BET surface areas of 1120, 460 and 705 $m^2\ g^{-1}$ with a pore sizes of 2.6, 2.3, and 2.2 nm for H-ImCOF, CH_3-ImCOF, and CF_3-ImCOF, respectively. Upon lithiation (treating with *n*-BuLi in hexane solution), the resultant R-Li-ImCOFs experienced significant porosity changes but remained crystalline. For example, H-Li-ImCOF in particular, possessed BET surface area of 350 $m^2\ g^{-1}$ and pore size of 2.9 nm. Having concentrated Li^+ ions in the pores, R-Li-ImCOFs were explored for lithium conduction. Remarkably, the solvated H-Li-ImCOF exhibited room-temperature lithium conductivity of 5.3×10^{-3} S cm^{-1}, while as high as 7.2×10^{-3} and 8.0×10^{-5} S cm^{-1} were achieved by CF_3-Li-ImCOF and CH_3-Li-ImCOF at

the same condition, respectively. Further analysis determined high t_{Li^+} values of 0.88, 0.93, and 0.81 were obtained by H-Li-ImCOF, CH_3-Li-ImCOF, and CF_3-Li-ImCOF, respectively. Compared to the previous COF-based lithium conductors mentioned previously (ICOF-2, CD-COF-Li and Li-CON-TFSI), the lithium conductivity of CF_3-Li-ImCOF was much superior, indicating the efficient lithium mobility within the framework of COFs. This remarkable conducting performance may due to the well-organization of the immobilized negatively-charge functional groups on the rigid backbone of the COFs, thus allowing for efficient mobility of loosely bound Li^+ ions as single-ion conductor. Came with similar concept, Lee and team prepared a lithium sulfonated COF (TpPa-SO_3Li) as solvent-free, single lithium-ion conductor.[171] The defined directional channel with anionic sulfonic acid moieties allowed for concentrated Li^+ ions to mobile efficiently. Interestingly, TpPa-SO_3Li could conduct lithium ions as high as 2.7×10^{-5} S cm^{-1} with very convincing t_{Li^+} value of 0.9 at room temperature. The high t_{Li^+} indicated the efficient transport of Li^+ ions within the channel of the COF.

Beside with ionic pendant groups, electroactive polymeric chain can also be set up in COFs as pendant groups that are compatible for concentrating Li^+ ions. In delight, poly(ethylene oxide) (PEO) and its derivatives which are widely employed as electrolyte, have been widely explored for LIBs owing to their high energy density, compatibility with lithium salts, safety, and easy assembly.[172–174] Thus, design of COFs with such electroactive polymeric chain could produce solid-sate lithium conductor with abundant active sites for Li^+ ions and defined channel for ion mobility. In the following report, lithium conductor COF (TPB-BMTP-COF) was designed by integrating flexible oligo(ethylene oxide) chains as pendant groups onto the pore walls.[175] TPB-BMTP-COF was crystalline material with BET surface area of 1746 m^2 g^{-1}, pore size of 3.02 nm and pore volume of 0.96 cm^3 g^{-1}. In addition, it exhibited high thermal stability (up to 300 °C). With the presence of oligo(ethylene oxide)

chains in the pores and its high porosity, as high as 4.3 wt% of Li^+ ions could be loaded on the pore of the COF upon diffusion of $LiClO_4$ to produce Li^+@TPB-BMTP-COF. For comparison, the previously reported TPB-DMTP-COF[176] (without oligo(ethylene oxide) chains instead of methoxy groups), was also prepared and further loaded with Li^+ ions (Li^+@TPB-DMTP-COF, 5.1 wt% of Li^+ ions loaded). Surface areas reduction were clearly observed for both resultant Li^+@COFs as consequence of high ion loading. Indeed, electronic absorption spectroscopy revealed that Li^+ ions were coordinatively interacted with the functional groups in both COFs. More importantly, both Li^+@COFs remained crystalline and exhibited sufficient thermal stability, signaling the well-preservation of the regular structures of the COFs even in the present of lithium salts. The lithium conductivity was then performed by preparing pellets and measured by alternating-current impedance spectroscopy. Interestingly, Li^+@TPB-BMTP-COF exhibited lithium conductivity as high as 6.04×10^{-6} and 1.66×10^{-4} S cm^{-1} at 40 and 80 °C, respectively, which were much higher than conducting performances of Li^+@TPB-DMTP-COF (1.36×10^{-7} and 5.37×10^{-6} S cm^{-1}) at similar conditions. These conducting enhancement was due to the presence of the polyelectrolyte chains aligned on the pore walls which could greatly promote the ion mobility. Indeed, TPB-BMTP-COF (with the absence of $LiClO_4$) was insulator under the same conductivity measurement. Recently, several COFs with electroactive polymeric chains have been bottom-up prepared for lithium conduction, such as $[TEO]_x$-TPB-DMTP-COFs, $[TEO]_x$-TPB-BMTP-COFs, $[TEO]_x$-TPB-BPTA-COFs, COF-POE-x-Li, PEG-Li^+@EB-COF-ClO_4, PEG-Li^+@CD-COF-Li, PEG-Li^+@COF-300, and PEG-Li^+@COF-5.[55,177,178] Meanwhile, postsynthetic incorporation of PEO or polyethylene glycol (PEG) into specific COFs (e.g., DBC-COFs) has also been demostrated to enhance the lithium conduvtivity of COFs.[179] All these designed COF-based lithium conductors clarify that COFs are robust materials for conductor applications.

3.4. Electroactive COFs for Fuel-Cells

As the increasing of global energy consumption, developing clean and renewable energy is in urgent demand.[180] Due to its high energy density, safety, and clean combustion, hydrogen fuel is one of promising energy technology for future renewable energy sources.[181,182] Specifically, fuel-cell technology such as hydrogen fuel-cell (HFC) or proton exchange membrane fuel cells (PEMFCs), offers a clean and reliable alternative energy source due to their high energy conversion efficiency, zero emissions, and mild operating conditions.[183] Hence, exploration of proton conducting materials usable for solid electrolyte membrane in PEMFCs has been in top of priority in this emerging field.[153] Considerably, the judicious fabrication of COFs membranes and thin films[184] and their tunable functional decoration with highly order and define pores[25,29,78], promise huge potential for exploration in fuel-cell technology. Indeed, COFs have been widely designed and explored for proton conduction as we briefly discussed in previous section.

Zamora and team utilized the previously reported imine-linked RT-COF-1[185] as potential solid electrolyte membrane in PEMFCs.[186] In the present work, the RT- COF-1 was doped with LiCl to produce LiCl@RT-COF-1 and further re-prepared using acetic acid instead of *m*-cresol to produce RT-COF-1Ac and RT-COF-1AcB (using glacial acetic acid) (**Figure 7**). RT-COF-1Ac possessed BET surface area of 750 $m^2 g^{-1}$ which was higher than both RT-COF-1 (330 $m^2 g^{-1}$) and RT-COF-1AcB (550 $m^2 g^{-1}$). Meanwhile, almost no surface area was recorded on LiCl@RT-COF-1 as consequence of LiCl occupation. Interestingly, the resultant LiCl@RT-COF-1 was crystalline and still manage high thermal stability, similar with its parent COF. More importantly, water uptake capability was enhanced in LiCl@RT-COF-1 (up to 635 $cm^3 g^{-1}$ at P/P_0 = 0.9, 90% RH)) relative to the RT-COF-1 and RT-COF-1Ac. This phenomenon is reasonable since Li^+ cations are highly hydrophilic.[187] Indeed, this uptake capability signals the potential application in proton conduction. Interestingly, LiCl@RT-COF-1, RT-COF-1Ac, and RT-COF-1AcB can be processed into compact films for ionic conductivity test. Remarkably, LiCl@RT-COF-1 film exhibited high proton conductivity of

6.45×10^{-3} S cm^{-1} at 313 K 100% RH, which was higher than both RT-COF-1AcB (5.25×10^{-4} S cm^{-1}) and RT-COF-1Ac (1.07×10^{-4} S cm^{-1}) films at the condition. This result showed the advantage of Li^+ cations in LiCl@RT-COF-1 for water uptake and proton conductivity. With high proton conductivities, all films were further employed as solid electrolyte membrane in PEMFC application. Accordingly, membrane electrode assembly (MEA) was designed with the COF films as solid electrolyte membrane and a commercial Pt/C catalyst (40 wt%) as both anode and cathode. Interestingly, the MEAs with different COF films displayed a starting open circuit potential (OCP or OCV) of 0.95, 0.88, and 0.42 V at 323 K for RT-COF-1Ac, RT-COF-1AcB, and LiCl@RT-COF-1 films, respectively. Nevertheless, the high OCV values signal for the good ionic conductivity and mechanical properties of the films for avoiding H_2 crossover. Further polarization and power density analysis showed that maximum power density of 12.95, 7.64, and 4.06 mW cm^{-2}, and maximum current density of 53.1, 45.9, and 54.5 mA cm^{-2} was achieved at 323 K by MEAs with RT-COF-1AcB, RT-COF-1Ac, and LiCl@RT-COF-1 films, respectively.

Meanwhile, on another occasion, Banerjee and team further tested the previously discussed super-protonic membranes-based COF (COFMs) as solid electrolyte membrane in real PEM device.[165] The COFMs were fabricated by slow baking of the building blocks in the presence of *p*-toluene sulfonic acid (PTSA.H_2O) and water at moderate temperature (50−90 °C), producing COFMs series (PTSA@TpBpy, PTSA@TpAzo and PTSA@TpBD$(Me)_2$). The resultant crystalline membranes possesed BET surface area ranging between 10–29 m^2 g^{-1}, while pore sizes of 2.8, 2.5, and 2.4 nm were shown by TpAzo, TpBpy, TpBD$(Me)_2$ after removal of PTSA, respectively. Intriguingly, the COFMs exhibited significantly high proton conductivity, such as as high as 7.8×10^{-2} S cm^{-1} at 80 °C for PTSA@TpAzo (under 95% RH), which was much superior among COF-based proton conductors (discusssed previously) and other crystalline porous organic polymer membranes (POPMs)-based proton conductors.[188,189] Meanwhile, as high as 6.2×10^{-2} and 5.3×10^{-2} S

cm^{-1} was achieved by PTSA@TpBpy and PTSA@TpBD(Me)$_2$, respectively. Having these remarkable proton conducting abilities, the COFMs were further explored in PEMFCs application by assembling and testing a single cell MEA. Notably, the single cell displayed an OCV of 0.81 V, a value that indicate the good ionic conductivity and mechanical properties of the film for avoiding H_2 crossover. On top of that, the cell delivered a maximum power output of 24 mW cm^{-2} (at 0.33 V) and a maximum current density of 90 mA cm^{-2} (at 0.20 V). Furthermore, the team also prepared another COF (bipyridine functionalized COF, TpBpy-MC) that was potential for as membrane in PEMFCs.[190] The TpBpy-MC synthesized via mechanosysthesis route can be transformed into more compact pellet compared to the powder COF obtained from traditional solvothermal route (TpBpy-ST). More importanly, after loading with phosphoric acid (H_3PO_4, PA), PA@TpBpy-MC in particular, exhibited a high proton conductivity of 2.5×10^{-3} S cm^{-1} (at 393 K). PA@TpBpy-MC was then employed as solid electrolyte membrane (pressed into pellet, ~850 μm) in PEFMCs under H_2/O_2 fuel-cell operating conditions. The assembled MEA (composed of PA@TpBpy-MC) showed OCV of 0.86 ± 0.02 and 0.90 V at 30 and 50 °C, respectively. In addition, the MEA delivered a maximum power density of 7 mW cm^{-2} and maximum curret density of 29 mA cm^{-2}.

Furthermore, by loading similar H_3PO_4, H_3PO_4@NKCOFs series were prepared and further used as solid electrolyte membrane in PEMFCs.[38] Interestingly, NKCOFs (NKCOF-1, -2, -3, -4) were highly crystalline materials featuring high chemical stability, such as stable in boiling water, strong acid (12 M HCl and 12 M H_3PO_4), and in base (12 M NaOH). In addition, the COFs posseseed high Langmuir surface areas (1011, 1510, 1139, and 2612 $m^2 g^{-1}$ for NKCOF-1, -2, -3, and -4 respectively). Structurically, NKCOFs possesed azo groups that allowed for efficient H_3PO_4 doping for extrinsic proton conductivity and phenolic groups that served as acid to directly donate protons for intrinsic proton conductivity. The presence of these groups along with their high surface areas, procure NKCOFs to be hydrophilic, hence supporting for loading H_3PO_4. Indeed, upon doping with H_3PO_4, the resultant

H_3PO_4@NKCOFs realized ultrahigh proton conductivity up to 1.13×10^{-1} S cm^{-1} (for H_3PO_4@NKCOF-1 at 353 K, 98% RH) which was the highest among all COF-based proton conductors. Additionally, their conducting abilities were maintained across a wide relative humidity (40–100%) and temperature ranges (20–80 °C). Having these remarkable proton conducting ability, H_3PO_4@NKCOFs were then employed as solid-state electrolyte membrane for PEMFCs application by preparing MEAs. Intriguingly, the MEAs afforded OCVs of 0.978, 0.953, 0.928, and 0.906 V for H_3PO_4@NKCOF-1, -2, -3, -4, respectively. Remarkably, H_3PO_4@NKCOF-1 achived notable maximum power density and current density up to 81 mW cm^{-2} and 456 mA cm^{-2}, respectively, which exceeded all previously reported COF-based MEAs discussed previously. Furthermore, a COF-based mixed matrix membrane, obtained by impregnation of a COF (H_3PO_4@SNW-1) into a Nafion matrix has also been reported elsewhere for PEMFCs application.[191] All these reports discussed in this sub-section exemplify the robust design of COFs for high conducting materials and their processable tranformed them into prospective solid-state membrane for PEMFCs. Although this field in COFs is still infancy, we have seen several remarkable results that vision the great prospects of utilization of COFs in fuel-cell technology.

3.5. Electroactive COFs for Electrocatalysis

Developing economic, environmentally friendly, and renewable energy storages and conversions technologies are one of the alternative solutions for the development of sustainable modern society.[192] Beside rechargeable batteries, electrocatalysis are one of the important technology for the efficient and green energy productions, such as for electrocatalytic CO_2 and O_2 reductions and water splitting technology (OER and HER).[39,193,194] In principle, electrocatalysis is a process that accelerate the electrochemical reactions occurred on the surface of electrode materials.[195] Practically, materials with abundant electrocatalytic sites, high surface area, high electrical conductivity, and profound

chemical and thermal stabilities are promising in electrocatalysis application.[193,196] Accordingly, highly stable porous materials, such as porous carbons and other related 2D materials have been widely explored for electrocatalysis application.[192,193] By virtue of the high porosity, high chemical and thermal stabilities, and yet, tuneable in incorporation of electroactive sites in COFs[25,27,52,197], they promise great prospects as electrocatalyst materials. In particular, design of COFs that able to confine electrocatalyst constituents (e.g., reactive metals) could transform COFs into potential electrocatalyst.[32,52,197,198] Recent reports have indicated the design and application of COFs in the field of electrocatalysis, such as in electrocatalytic CO_2 and O_2 reductions and water splitting (electrocatalytic OER and HER).

3.5.1. Electrocatalytic CO_2 Reduction

The electrochemical reduction of CO_2 into CO or other value-added products is essential chemical reaction to elevate the green-house effect and for efficient and effective clean energy production.[199] In 2015, Yaghi and team reported a seminal work in designing 2D COFs for electrocatalytic CO_2 reduction reaction (CO_2RR).[37] The COFs (COF-366-M and COF-367-M; M = Co or Co/Cu) were composed of electroactive cobalt porphyrin (Co-TAPP) units[200] which linked through covalent imine bonds. Structurally, the framework of the COFs constituted with catalytic cobalt and structural copper units. Hence, the COFs were highly active, stable, and selective catalyst for electrochemical CO_2RR into CO in water. The resultant COFs were highly crystalline and possessed high BET surface areas (1360 and 1470 $m^2\ g^{-1}$ for COF-366-Co and COF-367-Co, respectively). The presence of electroactive cobalt and the high surface areas call for potential application for electrocatalytic CO_2RR. Practically, the electrocatalytic CO_2RR was performed in CO_2-saturated aqueous bicarbonate buffer (pH = 7.3) solution under applied potentials between –0.57 and –0.97 V (*vs* RHE). Interestingly, CO was observed as the major reduction product. Furthermore, at –0.67 V, COF-366-Co could promote CO evolution as high as 36 ml (equivalent to 1.6 mmol at

STP)/mg of catalyst at an initial current density of 5 mA with Faradaic efficiency (FE_{CO}) of 90% and was extended for 24 h for producing similar volume of CO (36 mL). This corresponded to a turnover number (TON) of 1352 (or equivalent to (TON_{EA}) ≈34,000 per electroactive cobalt) with an initial turnover frequency (TOF) of 98 $hour^{-1}$(or equivalent to TOF_{EA} ≈ 2500 per electroactive cobalt). Interestingly, neither PXRD pattern changes nor Co NPs formation were observed after electrocatalysis experiment. Meanwhile, with larger surface area, COF-367-Co, could produce more than 100 mL of CO (or 4.5 mmol at STP)/mg of catalyst at similar voltage during 24 h. This corresponded to TON of 3901 (equivalent to TOF_{EA}= 48,000) with FE_{CO} of 91%. This activity enhancement clearly exemplifies the lattice expansion influenced the catalytic activity of the COF. Meanwhile, the bimetallic (Co/Cu) analog of this COF (COF-367-Co (10%) and COF-367-Co (1%)) were also prepared and further tested for similar electrocatalytic CO_2RR with slightly distinct performance. Further X-ray absorption data revealed this remarkable electrocatalytic activities arose from the COF environment on the electronic structure of the catalytic cobalt centers. Indeed, the results presented here compile that catalytic performances of COFs can be tuned at molecular level. Furthermore, the team further explored the effect of functional groups in COF-366-Co for overall electrocatalytic activities by preparing other *iso*-reticular structure analogs (COF-366-R-Co; R = -H, $-(OMe)_2$, -F or $-(F)_4$).[201] Interestingly, the catalytic activities were varied for all COF series, indicating the catalytic activity not only relied on the metal Co but also the chemical composition of the COFs.

On another occasion, 2D porphyrin-based COFs were again employed as catalyst to electrocatalytically reduce CO_2.[202] The COFs (M-TTCOFs) were composed of electroactive metalloporphyrin (M-TAPP, M = Co or Ni) and TTF units which arranged within layer-eclipsed structure (**Figure 8**). Meanwhile, TTF is a kind of electron donor species[203] that are able to stimulate charge-transfer within the crystal upon reacting with electron acceptor species such as metalloporphyrin.[204] Hence, TTF in M-TTCOFs could serve as electron

donator to construct an oriented electron transmission pathway with metalloporphyrin. The resultant M-TTCOFs were highly crystalline materials with BET surface areas of 675, 481 and 531 $m^2\ g^{-1}$ and pore volume of 0.612, 0.633, and 0.483 $cm^3\ g^{-1}$ for H_2-TTCOF, Co-TTCOF, and Ni-TTCOF, respectively. More importantly, the COFs exhibited notable CO_2 uptake, up to 20 $cm^3\ g^{-1}$ at 293 K for Co-TTCOF, which was higher than H_2-TTCOF (11 $cm^3\ g^{-1}$) and comparable with Ni-TTCOF (21 $cm^3\ g^{-1}$). These results confirmed that the presence of metals enhanced the CO_2 uptake. Furthermore, the COFs were chemically stable, even in water, 0.5 M $KHCO_3$ (pH = 7.2), 0.1 M HCl (pH = 1) and 0.1 M KOH (pH = 13). All these properties support M-TTCOFs as potential electrocatalyst for CO_2RR. Accordingly, the COFs were packed in cells and tested under three-electrode H-type cell with CO_2 or Ar-saturated 0.5 M $KHCO_3$ solution. Co-TTCOF exhibited higher current density (over −0.3 to −1.0 V *vs.* RHE) in CO_2-saturated $KHCO_3$ solution than that in Ar-saturated $KHCO_3$ solution, indicating the higher possibility of electrocatalytic CO_2RR than HER. In addition, both CO and H_2 were detected as the primary product without any liquid product detected. Interestingly, the Tafel slope of Co-TTCOF was 237 mV dec^{-1}, which was much smaller than Ni-TTCOF (629 mV dec^{-1}) and H_2-TTCOF (433 mV dec^{-1}), proving the more efficient CO kinetic production. Furthermore, Co-TTCOF could initially evolve CO at CO partial current density of 0.10 mA cm^{-2} (at −0.45 V) and exhibited maximum FE_{CO} of 91.3 % upon potential was increased to −0.7 V. Indeed, this FE_{CO} value was much higher than that of Ni-TTCOF (20.9%) and H_2-TTCOF (4.22%). Moreover, the TOF of Co-TTCOF was calculated as 1.28 s^{-1} at −0.7 V. interestingly, catalytic performance (in regards of FE_{CO}) of Co-TTCOF can be maintained > 90% even after 40 h testing, implying the highly stable electrocatalytic capability. Accordingly, the TON (for CO) was determined as high as 14,142 for 10 h and rose up to 141,479 after 40 h, while the TON (for H_2) rose from 4014 to 14,148 h at similar time course. Co-TTCOF was further exfoliated (Co-TTCOF NSs, thickness range of 5 to 6 nm) and tested for similar electrocatalytic test. Interestingly, Co-TTCOF NSs showed enhanced

electrocatalytic performance. For example, it exhibited maximum FE_{CO} of 99.7% at −0.8 V which was higher than that of Co-TTCOF (FE_{CO}, 91.3%). Furthermore, on another occasion, 3D COF (COF-300-AR) was also employed for electrocatalytic CO_2RR by specific structural design.[205] Indeed, this report shows that COFs can be further engineered as potential electrocatalysts under specific designed structures and compositions.

3.5.2. Electrocatalytic O_2 Reduction

Molecular oxygen is important as an ideal electron acceptor and has been widely studied in oxygen reduction reaction (ORR) in bioelectrochemical systems, such as enzymatic and microbial fuel cells and also in hydrogen fuel-cell technology.[206,207] COFs are interesting porous material for electrocatalyst since they are highly porous and tunable in functional decoration. Segura and team utilized naphthalene diimide-based COF (NDI-COF) as metal-free electrocatalyst for ORR.[208] NDI-COF was composed of electrochemically active naphthalene diimides (NDI) units that have been considered as promising electron acceptors[209], hence the backbone of the COF was energetically favourable to accept electrons from oxygen. NDI-COF possesssed BET surface area of 1138 $m^2\ g^{-1}$ and pore size of 2.5 nm. Furthermore, the COF was further exfoliated to obtain COF nanosheets (NDI-CONs) for better processing in preparing electrode for electrocatalytic ORR experiment. Practically, NDI-CON colloid was dropcasted on the glass-carbon electrode (NDI-CON/GC) and the eletrocatalytic test was performed using O_2-saturated 0.1 M NaOH solution as supporting electrolyte. The CV curves of NDI-CON/GC displayed O_2 reduction peak shifted toward more positive potential relative to the bare GC, indicating the ORR took place. With GC disk-Pt ring electrode, it was found that NDI-CON/GC exhibited lower onset potential (−0.25 V *vs.* SCE) compared to the bare GC electrode (−0.37 V *vs.* SCE) and showed potential shift of 120 mV toward positive potential. More importantly, the current was almost constant even after 10,000s, losing only *ca.* 3% relative to its initial value. Although the research on

electrocatalytic ORR using COFs is still infancy, the possible incorporation of metal catalyst such as Pt could enhance their electrocatalytic performance. For example, Pt and non-noble metal Cu have been incorporated in CTF compounds as electrocatalysts for ORR.[210,211] This fact exemplifies the huge potential of COFs as electrocatalysts for ORR.

3.5.3. Electrochemical Water Splitting

Electrochemical water splitting which involved HER and OER has been considered as an appealing route for sustainable production of green and renewable energies, such as hydrogen energy. So far, the noble metal platinum (Pt) is the most active element for HER, while noble metal oxides (IrO_x and RuO_x) are the benchmarked electrocatalysts for OER.[212] Furthermore, non-metal metal catalysts and metal-doped porous carbon materials have also been widely explored for water splitting to substitute those of noble metal catalyst.[196] In delight, with controlable composition and flexible incorporation of metal-catalyst,[52,78,198] COFs are promising materials for electrocatalytic water splitting application.

Oxygen Evolution Reaction (OER). By using Co instead of noble metal Pt, Banerjee and team design metal-COF electrocatalyst (Co-TpBpy) for OER.[213] The Co-TpBpy was fabricated by coordinatively intercalated the cobalt acetate on the bipyridine moieties of TpBpy. Accordingly, the metal doping clearly reduced the surface area of the host (from 1660 to 450 $m^2\ g^{-1}$). Since, Co-doped porous materials have been widely found able to catalyze the water oxidation reaction[214,215], Co-TpBpy is undoubtedly promising material for OER. In the prior electrochemical study of Co-TpBpy coated with glassy carbon electrode in 0.1 M aqueous phosphate buffer at pH 7, an overpotential of 400 mV was needed to achieve an anodic current density of 1 mA cm^{-2}. Further measurement confirmed Tafel slope of 59 mV $decade^{-1}$, which suggested the possible reversible one-electron transfer mechanism followed for OER. Notably, Co-TpBpy exhibited a TOF of 0.23 s^{-1} with faradaic efficiency (ε) of 0.95, signifying the excellence performance of Co-TpBpy as an OER catalyst. Furthermore, Co-

TpBpy showed efficient and stable electrocatalytic OER performance, retaining 94% of its OER activity even after 1000 cycles.

Tomas and team further engineered the morphology and porosity of TpBpy into micro/macroporous material (macro-TpBpy) before doping with Co.[216] The resultant macro-TpBpy possessed interconnected macropores structures while maintaining its crystallinity and chemical stability. Upon doping with Co, macro-TpBpy-Co could provide fast mass and ion transport into to hierarchical structures which is highly desirable, particularly for a diffusion-limited process such as for OER. The resultant macro-TpBpy-Co was then employed as electrocatalyst for OER using alkaline aqueous electrolyte (0.1 M KOH) in the typical three-electrode system. In the initial measurement, macro-TpBpy-Co exhibited an overpotential of 380 mV (*vs* RHE) to achieve an anodic current density of 10 mA cm^{-2}, which was much lower than that of macro-TpBpy and TpBpy-Co. Interestingly, it documented an overpotential of only 430 mV (at 50 mA cm^{-2}), which was 170 mV lower than the benchmark RuO_2 catalyst. Furthemrore, macro-TpBpy-Co and TpBpy-Co exhibited Tafel slope of 54 and 58 mV dec^{-1}, respectively, which were much lower than that of macro-TpBpy (339 mV dec^{-1}) and RuO_2 (79 mV dec^{-1}), indicating favorable reaction kinetics in the OER process in the presence of Co. In addition, a Faradaic efficiency as high as ~98% was obtained by macro-TpBpy-Co for OER in 0.1 M KOH, signifying the high catalytic activity of macro-TpBpy-Co. These remarkable electrocatalytic performances may arise from the improved mass diffusion properties in the hierarchically porous COF structures, together with the easily accessible active Co^{2+}-bipyridine sites. Meanwhile, reticulating COF structures by controlling elemental composition such as CN stoichiometry and N position could also transformed COFs into promising metal-free electrocatalyst for OER , such as the reported phenazine-linked COF-C_4N.[217] All these reports describe the feasibility of COF as promising OER electrocatalyst by structural composition tuning.

Hydrogen Evolution Reaction (HER). Similar with electrocatalytic OER, COFs have also been employed as electrocatalyst for HER. For example, a predesigned COF composed of electroactive porphyrin and pyrene could be potential for electrocatalytic application.[218] In delight, a pyrene-porphyrin based 2D COF (SB-PORPy-COF) was designed as potential metal-free electrocatalyst for HER.[219] SB-PORPy-COF was synthesized by condensing 5,10,15,20-tetrakis(4-aminophenyl)porphyrin (TAP) and 1,3,6,8-tetrakis (4-formylphenyl) pyrene (TFFPy) to afford COF with porphyrin and pyrene units. The resultant COF was crystalline, chemically stable and possessed permanent microporosity (1.7 nm) with BET surface area of ~869 $m^2 g^{-1}$. SB-PORPy-COF was then employed as metal-free electrocatalyst for HER. Accordingly, the electrocatalytic test was performed in acidic (0.5 M H_2SO_4) solution. Notably, SB-PORPy exhibited a remarkable low onset overpotential of ~50 mV, which was the lowest reported overpotential for any types of COF electrocatalysts in acidic solution. Meanwhile, it showed relatively low overpotential (380 mV) to achieve 5 mA cm^{-2} exchange current density, proving the remarkable catalytic activity toward HER in term of COF-based system. In addition, SB-PORPy exhibited Tafel slope of ~116 mV dec^{-1}. More importantly, the electrocatalytic activity of SB-PORPy could be maintained for 500 cycles at scan rate of 100 mV s^{-1} in the potential range 0.2 V to −0.5 V (*vs* RHE). Nevertheless, it exhibited Faradaic efficiency as high as 90%, signifying the high selective of the catalyst toward hydrogen evolution. Although the report on COFs in this field is still rare, this report could not only enrich the structural diversity of COFs, but also provide understanding of the electrochemical behaviors (especially HER) of COFs and may inspire for the next incoming reports.

4. Conclusions and Perspectives

COFs as an emerging class of porous crystalline materials exhibit controllable chemical compositions, porosities, topologies and profound chemical stabilities. The synthesis of COFs

allows for precise integration of building blocks with varied compositions and functions into repetitive structures. Hence, the design of COFs provides judicious controlled of structure-function relationships. This includes the flexible design of electroactive COFs that are potential for energy-related applications such as in the field of electrochemical energy storages (e.g., capacitors and batteries), electrochemical energy generation (e.g., ORR, OER, HER and fuel-cell), electrical/ionic conductors and electrocatalysis. So far, the design of electroactive COFs encompasses the design of 1) bulk or exfoliated COFs to allow efficient ions/charges storage and mobility and also easy electrode processing; 2) COFs with electroactive skeletons by condensing electroactive building blocks or generating reactive skeletons during reticulation; 3) COFs with electroactive functional groups such as by installing electron rich/or electron deficient functional groups in COF skeletons; 4) electroactive COFs by doping redox active or catalytically active metals; and 5) electroactive COF hybrids by compositing of COFs with other conductive or electroactive components.

Several advances have been made in the design of electroactive COFs and remarkable performances in the field of electrochemical energy storages and generation, electrical/ionic conductors, and electrocatalysis have been obviously seen. For example, some exfoliated COFs and bulk COFs (self-standing film or polymer/COF hybrids) have been prepared and succesfully been integrated into devices for capacitor and battery applications. Similarly, various kind of pristine and COF hybrids (e.g., COF@CNT) have been widely employed as active materials for rechargeable metal-ion batteries with superior capacity and notable cycling stability. Meanwhile, in the field of electrical and ion conductors, several COFs have shown remarkable electrical and ionic conductivities, including the utilization of 3D COFs with high surface areas (3D-TTF-COFs). In addition, in the field of fuel-cell technology, several 2D COF membranes have been prepared and integrated into the MEA devices. Interestingly, some of them (e.g., H_3PO_4@NKCOFs) could even showed notable proton conductivity (1.13×10^{-1} S cm^{-1}) and significantly high power and current densities (up to 81

mW cm^{-2} and 456 mA cm^{-2}, respectively). Meanwhile, in the field of electrocatalyst, some 2D COFs (e.g., COF-367-M) could reduce CO_2 in very high TON (3901) and TOF (48,000) and exhibited high faradaic efficiency (91%). All these remarkable performances arise from the well-tuned structural composition, high structural order with well-defined porosities and high thermal and chemical stabilities in COFs.

Despite significant progresses have been devoted, the exploration of electroactive COFs is still infancy. Indeed, several technical challenges for future development of electroactive COFs are still need progressive attentions. For example, the employment of COFs as active materials for EDLC electrodes are still in the beginning. Although COFs can be prepared with high surface areas and excellent thermal and chemical stabilities, they are generally less-conductive. Hence, the development of highly conductive COFs (e.g., introduction electroactive building blocks or incorporation of conductive components) is paramount in preparing COF-based EDCLs. Furthermore, engineering COFs into nanostructures, such as layer exfoliation treatment, could enhance the accessible active surfaces while exposing more active sites. Such effort is also practical in designing COFs as electrode materials for batteries. Furthermore, tuning the chemical compositions of COFs, such as introduction of heteroatoms (N, S, O and B) is also powerful to enhance the electrochemical behavior (conductivity, capacitance, power and energy densities). Accordingly, COFs with highly dense heteroatoms are interesting to develop, such as benzoxazole and phenazine-linked COFs. Indeed, compositing COFs with graphene, CNTs or other conductive and electroactive polymers have also been seen to enhance the electrochemical activities. Meanwhile, exploration of electroactive COFs for metal-ion batteries (especially in SIB, ZIBs, and PIBs) is still less-explored compared to LIBs. Thus, developing COFs for metal-ion batteries is emergent. Technically, designing COFs that are able to attract Na^+, Zn^{2+}, and K^+ ions can be a perfect solution to develop those metal-ion batteries. Similarly, COFs can be explored more for possibility to conduct other metal ions such as Na^+, K^+, Mg^{2+}, or Al^{3+} by specific structural

design. Special attention to fuel-cell technology, preparing COF membranes with well-tuned anisotropic direction and crack-free with controlled thickness will enhance the protonic conductivity and mechanical properties, thus improved hydrogen energy generation. The exploitation of COFs in water splitting application, especially in electrocatalytic HER is the one of the most recently explored. Great prospects are clearly expected for COFs in HER, such as designing COFs with reactive metals (Pt or other reactive non-noble metals).

We believed that the tailorable chemical compositions, porosities and profound chemical and thermal stabilities of COFs are important driving forces to engineer them as prospective electroactive materials for energy-related applications. The highly enthusiastic of researchers toward this emerging porous material will generate innovative and upgrade porous materials for developing smart materials.

Acknowledgements

This work was supported by National Natural Science Foundation of China (21571079, 21621001, 21390394, 21571076, and 21571078), ″111″ project (B07016 and B17020), and the program for JLU Science and Technology Innovative Research Team. Q.F. and V.V. acknowledge the Thousand Talents program (China).

Conflict of Interest

The authors declare no conflict of interest.

Received: ((will be filled in by the editorial staff))
Revised: ((will be filled in by the editorial staff))
Published online: ((will be filled in by the editorial staff))

References

[1] M. G. Walter, E. L. Warren, J. R. McKone, S. W. Boettcher, Q. Mi, E. A. Santori, N. S. Lewis. *Chem. Rev.* **2010**, *110*, 6446.

[2] J. B. Goodenough. *Energy. Environ. Sci.* **2014**, *7*, 14

[3] I. Roger, M. A. Shipman, M. D. Symes. *Nat. Rev. Chem.*, **2017**, *1*, 003

[4] X. Zou, Y. Zhang, *Chem. Soc. Rev.* **2015**, *44*, 5148.

[5] H. B. Gray. *Nat. Chem.* **2009**, ***1***, 7.

[6] Y. Lee, J. Suntivich, K. J. May, E. E. Perry, Y. Shao-Horn, *J. Phys. Chem. Lett.* **2012,** *3*, 399.

[7] A. Walcarius, *Chem. Soc. Rev.* **2013,** *42*, 4098.

[8] T. B. Schon, B. T. McAllister, P. F. Li, D. S. Seferos. *Chem. Soc. Rev.* **2016**, *45*, 6345.

[9] J. Xie, P. Gu, Q. Zhang. *ACS Energy Lett.* **2017**, *2*, 1985.

[10] K. Mitsudo, Y. Kurimoto, K. Yoshioka, S. Suga. *Chem. Rev.* **2018**, *118*, 5985.

[11] W. Xin, Y. Song. *RSC Adv.* **2015,** *5*, 83239.

[12] W. J. Roth, P. Nachtigall, R. E. Morris, J. Čejka. *Chem. Rev.* **2014,** *114*, 4807.

[13] D. R. Rolison, C. A. Bessel. *Acc. Chem. Res.* **2000,** *33*, 737.

[14] M. Severance, Y. Zheng, E. Heck, P. K. Dutta. *J. Phys. Chem. A* **2013,** *117*, 13704.

[15] F.-Y. Yi, R. Zhang, H. Wang, L. -F. Chen, L. Han, H. -L. Jiang, Q. Xu. *Small Methods* **2017**, *1*, 1700187.

[16] A. Morozan, F. Jaouen. *Energy Environ. Sci.* **2012**, *5*, 9269.

[17] W. Zheng, M. Liu, L. Y. S. Lee. *ACS Catal.* **2019**, *10*, 81.

[18] H. Furukawa, K. E. Cordova, M. O'Keeffe, O. M. Yaghi. *Science* **2013**, *9*, 1230444.

[19] N. Kornienko, Y. Zhao, C. S. Kley, C. Zhu, D. Kim, S. Lin, C. J. Chang, O. M. Yaghi, P. Yang. *J. Am. Chem. Soc.* **2015**, *137*, 14129.

[20] Y. Yoshida, H. Kitagawa. *ACS Sustain. Chem. Eng.* **2019**, *7*, 70.

[21] S. Samanta, S. Khilari, K. Bhunia, D. Pradhan, B. Satpati, R. Srivastava. *J. Phys. Chem. C* **2018**, *122*, 10725.

[22] J. Milikić, M. Vasić, L. Amaral, N. Cvjetić, D. Jugović, R. Hercigonja, B. Šljukić. *Int. J. Hydrogen Energy* **2018**, *43*, 18977.

[23] A. P. Côté, N. W. Ockwig, A. P. Cote, M. O. Keeffe, A. J. Matzger, O. M. Yaghi. *Science* **2005**, *310*, 1166.

[24] X. Feng, X. Ding, D. Jiang. *Chem. Soc. Rev.* **2012**, *41*, 6010.

[25] S.-Y. Ding, W. Wang, *Chem. Soc. Rev.* **2013**, *42*, 548.

[26] X. Y. Guan, F. Q. Chen, Q. R. Fang, S. L. Qiu. *Chem. Soc. Rev.* **2020**, DOI: 10.1039/c9cs00911f.

[27] P. J. Waller, F. Gándara, O. M. Yaghi. *Acc. Chem. Res.* **2015**, *48*, 3053.

[28] N. Huang, P. Wang, D. Jiang. *Nat. Rev. Mater.* **2016**, *1*, 16068.

[29] Y. Yusran, X. Y. Guan, H. Li, Q. R. Fang, S. L. Qiu. *Nat. Sci. Rev.* **2019**, *7*, 170.

[30] Y. Yusran, Q. R. Fang, S. L. Qiu. *Isr. J. Chem.* **2018**, *58*, 971.

[31] Z. Xiang, D. Cao. *J. Mater. Chem. A* **2013**, *1*, 2691.

[32] M. Dogru, T. Bein. *Chem. Commun.* **2014**, *50*, 5531.

[33] J. L. Segura, M. J. Mancheño, F. Zamora, *Chem. Soc. Rev.* **2016**, *45*, 5635.

[34] Y. Yusran, H. Li, X. Y. Guan, D. H. Li, L. X. Tang, M. Xue, Z. B. Zhuang, Y. S. Yan, V. Valtchev, S. L. Qiu, Q. R. Fang. *Adv. Mater.* **2020**, *32*, 1907289.

[35] H. Li, J. H. Chang, S. S. Li, X. Y. Guan, D. H. Li, C. Y. Li, L. X. Tang, M. Xue, Y. S. Yan, V. Valtchev, S. L. Qiu, Q. R. Fang. *J. Am. Chem. Soc.* **2019**, *141*, 13324.

[36] B. Q. Li, S. Y. Zhang, B. Wang, Z. J. Xia, C. Tang, Q. Zhang. *Energy Environ. Sci.* **2018**, *11*, 1723.

[37] S. Lin, C. S. Diercks, Y. -B. Zhang, N. Kornienko, E. M. Nichols, Y. Zhao, A. R. Paris, D. Kim, P. Yang, O. M. Yaghi, C. J. Chang. *Science*, **2015**, *349*, 1208.

[38] Y. Yang, X. He, P. Zhang, Y. H. Andaloussi, H. Zhang, Z. Jiang, Y. Chen, Sh. Ma, P. Cheng, Z. Zhang. *Angew. Chem. Int. Ed.* **2019**, DOI: 10.1002/anie.201913802

[39] S. Ghosh, R. N. Basu, *Nanoscale* **2018**, ***10***, 11241.

[40] A. Halder, M. Ghosh, A. M. Khayum, S. Bera, M. Addicoat, H. S. Sasmal, S. Karak, S. Kurungot, R. Banerjee. J. *Am. Chem. Soc.* **2018**, *140*, 10941.

[41] D. -G. Wang, N. Li, Y. Hu, S.Wan, M. Song, G. Yu, Y. Jin, W. Wei, K. Han, G. -C. Kuang, W.bZhang. *ACS Appl. Mater. Interfaces* **2018**, *10*, 42233.

[42] X. -C. Li, Y. Zhang, C. -Y. Wang, Y. Wan, W. -Y. Lai, H. Pang, W. Huang. *Chem. Sci.* **2017**, *8*, 2959.

[43] Q. Xu, S. Tao, Q. Jiang, D. Jiang, *J. Am. Chem. Soc.* **2018**, *140*, 7429.

[44] F. Xu, S. Jin, H. Zhong, D.Wu, X. Yang, X. Chen, H. Wei, R. Fu, D.Jiang. *Sci. Rep.* **2015**, *5*, 8225.

[45] Z. Luo, L. Liu, J. Ning, K. Lei, Y. Lu, F. Li, J. Chen. *Angew. Chem. Int. Ed.* **2018**, *57*, 9443.

[46] S. Wang, Q. Wang, P. Shao, Y. Han, X. Gao, L. Ma, S.Yuan, X. Ma, J. Zhou, X. Feng, B. Wang. *J. Am. Chem. Soc.* **2017**, *139*, 4258.

[47] S. Chandra, T. Kundu, S. Kandambeth, R. BabaRao, Y. Marathe, S. M. Kunjir, R. Banerjee. *J. Am. Chem. Soc.* **2014**, *136*, 6570.

[48] A. M. Sanchez, M. Barra, R. H. De Rossi, *J. Org. Chem.* **1999**, *64*, 1604.

[49] R. Shi, L. Liu, Y. Lu, C. Wang, Y. Li, L. Li, Z. Yan, J. Chen. *Nat. Commun.* **2020**, *11*, 178.

[50] Y. Du, H. Yang, J. M. Whiteley, S. Wan, Y. Jin, S. -H. Lee, W. Zhang. *Angew. Chem. Int. Ed.* **2016**, *55*, 1737.

[51] H. Chen, H. Tu, C. Hu, Y. Liu, D. Dong, Y. Sun, Y. Dai, S. Wang, H. Qian, Z. Lin, L. Chen. *J. Am. Chem. Soc.* **2018**, *140*, 896.

[52] J. L. Segura, S. Royuela, M. M. Ramos. *Chem. Soc. Rev*. **2019**, *48*, 3903.

[53] M. S. Lohse, T. Bein. *Adv. Funct. Mater.* **2018**, *28*, 1705553.

[54] Y. Peng, G. Xu, Z. Hu, Y. Cheng, C. Chi, D. Yuan, H. Cheng, D. Zhao. *ACS Appl. Mater. Interfaces* **2016**, *8*, 18505.

[55] G. Zhang, Y. L. Hong, Y. Nishiyama, S. Bai, S. Kitagawa, S. Horike. *J. Am. Chem. Soc.* **2019**, *141*, 1227.

[56] J. F. Vélez, M. Aparicio, J. Mosa. *J. Phys. Chem. C* **2016**, *120*, 22852.

[57] Y. Kato, K. Hasumi, S. Yokoyama, T. Yabe, H. Ikuta, Y. Uchimoto, M. Wakihara. *Solid State Ionic* **2002**, *150*, 355.

[58] A. M. Khayum, M. Ghosh, V. Vijayakumar, A. Halder, M. Nurhuda, S. Kumar, M. Addicoat, S. Kurungot, R.Banerjee. *Chem. Sci.* **2019**, *10*, 8889.

[59] Z. Guo, Y. Ma, X. Dong, J. Huang, Y. Wang, and Y. Xia, *Angew. Chem. Int. Ed.* **2018**, *57*, 11737.

[60] F. Wan, L. Zhang, X. Wang, S. Bi, Z. Niu, J. Chen. *Adv. Funct. Mater.* **2018**, *28*, 1804975.

[61] W. Long, B. Fang, A. Ignaszak, Z. Wu, Y. J. Wang, D. Wilkinson. *Chem. Soc. Rev.* **2017**, *46*, 7176.

[62] Y. Yang, C. Wang, B. Yue, S. Gambhir, C. O. Too, and G. G. Wallace. *Adv. Energy Mater.* **2012**, *2*, 266.

[63] F. Xu, X. Chen, Z. Tang, D. Wu, R. Fu, D. Jiang. *Chem. Commun.* **2014**, *50*, 4788.

[64] Y. Luo, R. Guo, T. Li, F. Li, Z. Liu, M. Zheng, B. Wang, Z. Yang, H. Luo, Y. Wan. *ChemSusChem* **2019**, *12*, 1591.

[65] S. Zhang, W. Guo, F. Yang, P. Zheng, R. Qiao, Z. Li. *Batter. Supercaps* **2019**, *2*, 627.

[66] C. Li, Z. Xi, D. Guo, X. Chen, L. Yin. *Small* **2018**, *14*, 1701986.

[67] Z. Lei, Q. Yang, Y. Xu, S. Guo, W. Sun, H. Liu, L. -P. Lv, Y. Zhang, Y. Wang. *Nat. Commun.* **2018**, *9*, 576.

[68] Z. A. Ghazi, L. Zhu, H. Wang, A. Naeem, A. M. Khattak, B. Liang, N. A. Khan, Z. Wei, L. Li, Z. Tang. *Adv. Energy Mater.* **2016**, *6*, 1601250.

[69] F. Bu, I. Shakir, Y. Xu, *Adv. Mater. Interfaces* **2018**, *5*, 1800468.

[70] J. Liu, J. Wang, C. Xu, H. Jiang, C. Li, L. Zhang, J. Lin, Z. X. Shen. *Adv. Sci.* 2018, 5, 201700322.

[71] P. J. Hall, M. Mirzaeian, S. I. Fletcher, F. B. Sillars, A. J. R. Rennie, G. O. Shitta-Bey,

G. Wilson, A. Cruden, R. Carter. *Energy Environ. Sci.* **2010**, *3*, 1238.

[72] Y. Wang, Y. Song, Y. Xia. *Chem. Soc. Rev.* **2016**, *45*, 5925.

[73] D. Pech, M. Brunet, H. Durou, P. Huang, V. Mochalin, Y. Gogotsi, P. -L. Taberna, P. Simon. *Nat. Nanotechnol.* **2010**, *5*, 651.

[74] W. Gao, N. Singh, L. Song, Z. Liu, A. L. M. Reddy, L. Ci, R. Vajtai, Q. Zhang, B.Wei, P. M. Ajayan. *Nanotechnol.* **2011**, *6, 496.*.

[75] A. F. M. El-Mahdy, Y. H. Hung, T. H. Mansoure, H. H. Yu, T. Chen, S. -W. Kuo. *Chem. Asian J.* **2019**, *14*, 1429.

[76] A. F. M. EL-Mahdy, M. G. Mohamed, T. H. Mansoure, H. -H. Yu, T. Chen, S.-W. Kuo. *Chem. Commun.* **2019**, *55*, 14890.

[77] S. B. Alahakoon, C. M. Thompson, G. Occhialini, R. A. Smaldone. *ChemSusChem* **2017**, *10*, 2116.

[78] K. Geng, T. He, R. Liu, K. T. Tan, Z. Li, S. Tao, Y. Gong, Q. Jiang, D. Jiang. *Chem. Rev.* **2020**, DOI: 10.1021/acs.chemrev.9b00550

[79] J. Zhou, B. Wang, *Chem. Soc. Rev.* **2017**, *46*, 6927.

[80] C. R. Deblase, K. E. Silberstein, T. T. Truong, H. D. Abruña, W. R. Dichtel, *J. Am. Chem. Soc.* **2013**, *135*, 16821.

[81] B. Hu, J. Luo, M. Hu, B. Yuan, T. L. Liu. *Angew. Chem. Int. Ed.* **2019**, *58*, 16629.

[82] C. R. Mulzer, L. Shen, R. P. Bisbey, J. R. McKone, N. Zhang, H. D. Abruña, W. R. Dichtel. *ACS Cent. Sci.* **2016**, *2*, 667.

[83] M. A. Khayum, V. Vijayakumar, S. Karak, S. Kandambeth, M. Bhadra, K. Suresh, N. Acharambath, S. Kurungot, R. Banerjee. *ACS Appl. Mater. Interfaces* **2018**, *10*, 28139.

[84] C. Singh,, A. Paul. *J. Phys. Chem. C* **2015**, *119*, 11382.

[85] S. Chandra, D. Roy Chowdhury, M. Addicoat, T. Heine, A. Paul, R. Banerjee. *Chem. Mater.* **2017**, *29*, 2074.

[86] Y. Zhang, L. Tao, C. Xie, D. Wang, Y. Zou, R. Chen, Y. Wang, C. Jia, S. Wang. *Adv.*

Mater. **2020**, DOI: 10.1002/adma.201905923.

[87] F. Cheng, J. Liang, Z. Tao, J. Chen. *Adv. Mater*. **2011**, *23*, 1695.

[88] Y. Sun, N. Liu, . Y. Cui. *Nat. Energy* **2016**, *1*, 16071.

[89] M. Li, J. Lu, Z. Chen, K. Amine. *Adv. Mater*. **2018**, *30*, 1800561.

[90] Y. Liang, Z. Tao, J. Chen. *Adv. Energy Mater.* **2012**, *2*, 742.

[91] C. Peng, G. -H. Ning, J. Su, G. Zhong, W. Tang, B. Tian, C. Su, D. Yu, L.Zu, J. Yang, M. -F. Ng, Y. -S. Hu, Y. Yang, M. Armand, K. P. Loh. *Nat. Energy* **2017**, *2*, 17074.

[92] L. M. Zhu, A. W. Lei, Y. L. Cao, X. P. Ai, H. X. Yang. *Chem. Commun.* **2013**, *49*, 567.

[93] T. M. Gür. *Energy Environ. Sci.* **2018**, *11*, 2696.

[94] S. Wu, W. Wang, M. Li, L. Cao, F. Lyu, M. Yang, Z. Wang, Y. Shi, B. Nan, S. Yu, Z. Sun, Y. Liu, Z. Lu. *Nat. Commun.* **2016**, *7*, 13318.

[95] S. Xu, G. Wang, B. P. Biswal, M.Addicoat, S. Paasch, W. Sheng, X. Zhuang, E. Brunner, T. Heine, R. Berger, X. Feng. *Angew. Chem. Int. Ed.*, **2019**, *58*, 849.

[96] Y. Liu, X. Zhao, C. Fang, Z. Ye, Y. -B. He, D. Lei, J. Yang, Y. Zhang, Y. Li, Q. Liu, Y. Huang, R. Zeng, L. Kang, J. Liu, Y. -H. Huang. *Chem* **2018**, *4*, 2463.

[97] V. Palomares, P. Serras, I. Villaluenga, K. B. Hueso, J. Carretero-González, T. Rojo, *Energy Environ. Sci.* **2012**, *5*, 5884.

[98] S. W. Kim, D. H. Seo, X. Ma, G. Ceder, K. Kang. *Adv. Energy Mater.* **2012**, *2*, 710.

[99] S. Komaba, T. Hasegawa, M. Dahbi, K. Kubota. *Electrochem. Commun.* **2015**, *60*, 172.

[100] G. Fang, J. Zhou, A. Pan, S. Liang. *ACS Energy Lett.* **2018**, *3*, 2480.

[101] Y. -G. Guo, J. -S. Hu, and L. -J. Wan. *Adv. Mater.* **2008**, *20*, 2878.

[102] S. Muench, A. Wild, C. Friebe, B. Häupler, T. Janoschka, and U. S. Schubert. *Chem. Rev.* **2016**, *116*, 9438.

[103] J. L. Segura, R. Juárez, M. Ramos, and C. Seoane, *Chem. Soc. Rev.* **2015**, *44*, 6850.

[104] D. -H. Yang, Z. -Q. Yao, D. Wu, Y. -H. Zhang, Z. Zhou, and X. -H. Bu, *J. Mater. Chem. A* **2016**, *4*, 18621.

[105] D. Chen, A. -J. Avestro, Z. Chen, J. Sun, S. Wang, M. Xiao, Z. Erno, M. M. Algaradah, M. S. Nassar, K. Amine, Y. Meng, J. F. Stoddart. *Adv. Mater.* **2015**, *27*, 2907.

[106] Z. Wang, Y. Li, P. Liu, Q. Qi, F. Zhang, G. Lu, X. Zhao, X. Huang. *Nanoscale* **2019**, *11*, 5330.

[107] A. Ponrouch, E. Marchante, M. Courty, J. M. Tarascon, M. R. Palacín. *Energy Environ. Sci.* **2012**, *5*, 8572.

[108] B. C. Patra, S. K. Das, A. Ghosh, K. A.Raj, P. Moitra, M. Addicoat, S. Mitra, A. Bhaumik, S. Bhattacharya, A. Pradhan. *J. Mater. Chem. A* **2018**, *6*, 16655.

[109]J. C. Pramudita, D. Sehrawat, D. Goonetilleke, N. Sharma. *Adv. Energy Mater.* **2017**, *7*, 1602911.

[110] D. Kundu, B. D. Adams, V. Duffort, S. H. Vajargah, L. F. Nazar. *Nat. Energy* **2016**, *1*, 16119.

[111] P. Canepa, G. S. Gautam, D. C. Hannah, R. Malik, M. Liu, K. G. Gallagher, K. A. Persson, G. Cede. *Chem. Rev.* **2017**, *117*, 4287.

[112] Q. Zhao, W. Huang, Z. Luo, L. Liu, Y. Lu, Y. Li, L. Li, J. Hu, H. Ma, J. Chen. *Sci. Adv.* **2018**, *4*, eaao1761.

[113] X. Chen, H. Zhang, C. Ci, W. Sun, Y. Wang. *ACS Nano* **2019**, *13*, 3600.

[114] L. Chen, G. Shi, J. Shen, B. Peng, B. Zhang, Y. Wang, F. Bian, J. Wang, D. Li, Z. Qian, G. Xu, G. Liu, J. Zeng, L. Zhang, Y. Yang, G. Zhou, M. Wu, W. Jin, J. Li, H. Fang. *Nature* **2017**, *550*, 380.

[115] G. Shi, L. Chen, Y. Yang, D. Li, Z. Qian, S. Liang, L. Yan, L. H. Li, M. Wu, H. Fang. *Nat. Chem.* **2018**, *10*, 776.

[116] D. Larcher, J. -M. Tarascon. *Nat. Chem.* **2015**, *7*, 19.

[117] A. Manthiram, Y. Fu, Y. -S. Su. *Acc. Chem. Res.* **2013**, *46*, 1125.

[118] A. Manthiram, Y. Fu, S. -H. Chung, C. Zu, Y. -S. Su. *Chem. Rev.* **2014**, *114*, 11751.

[119] J. Wang, Y. -S. He, J. Yang. *Adv. Mater.* **2015**, *27*, 569.

[120] Y. Diao, K. Xie, S. Xiong, X. Hong, *J. Power Sources* **2013**, *235*, 181.

[121] C. -P. Yang, Y. -X. Yin, H. Ye, K. -C. Jiang, J. Zhang, Y. -G. Guo. *ACS Appl. Mater. Interfaces* **2014**, *6*, 8789.

[122] H. Liao, H. Ding, B. Li, X. Ai, C. Wang. *J. Mater. Chem. A* **2014**, *2*, 8854.

[123] J. Yoo, S. -J. Cho, G. Y. Jung, S. H. Kim, K. -H. Choi, J. -H. Kim, C. K. Lee, S. K. Kwak, S. -Y. Lee. *Nano Lett.* **2016**, *16*, 3292.

[124] Q. Xu, K. Zhang, J. Qian, Y. Guo, X. Song, H. Pan, D.Wang, X. Li. *ACS Appl. Energy Mater.* **2019**, *2*, 5793.

[125] Z. Xie, X. Zhang, Z. Zhang, Z. Zhou. *Adv. Mater.* **2017**, *29*, 160581.

[126] W. Zhang, Y. Huang, Y. Liu, L. Wang, S. Chou, H. Liu. *Adv. Energy Mater*. **2019**, *9*, 1900464.

[127] X. Mu, H. Pan, P. He, H. Zhou. *Adv. Mater.* **2019**, doi: 10.1002/adma.201903790.

[128] J. -S. Lee, S. T. Kim, R. Cao, N. -S. Choi, M. Liu, K. T. Lee, J. Cho. *Adv. Energy Mater*. **2011**, *1*, 34.

[129] Q. Sun, Y. Yang, Z. -W. Fu. *Electrochem. commun.* **2012**, *16*, 22.

[130] T. Ogasawara, A. Débart, M. Holzapfel, P. Novák, P. G. Bruce. *J. Am. Chem. Soc.* **2006**, *128*, 1390.

[131] X. Li, H. Wang, Z. Chen, H. -S. Xu, W. Yu, C. Liu, X. Wang, K. Zhang, K. Xie, K. P. Loh. *Adv. Mater.* **2019**, *31*, 1905879.

[132] S. Yang, Y. Qiao, P. He, Y. Liu, Z. Cheng, J. -J. Zhu, H. Zhou. *Energy Environ. Sci.* **2017**, *10*, 972.

[133] A. Kamyshny, S. Magdassi. *Chem. Soc. Rev.* **2019**, *48*, 1712.

[134] H. -N. Wang, X. Meng, L. -Z. Dong, Y. Chen, S. -L. Li, Y. -Q. Lan. *J. Mater. Chem. A* **2019**, *7*, 24059.

[135] S. Duhović, M. Dincă. *Chem. Mater.* **2015**, *27*, 5487.

[136] S. Wan, J. Guo, J. Kim, H. Ihee, D. Jiang. *Angew. Chem. Int. Ed.* **2008**, *47*, 8826.

[137] A. A. Talin, A. Centrone, A.C. Ford, M.E. Foster, V. Stavila, P. Haney, R. A. Kinney, V. Szalai, F. E. Gabaly, H. P. Yoon, F. Léonard, M. D. Allendorf. *Science* **2014**, *343*, 66.

[138] S. -L. Cai, Y. -B. Zhang, A. B. Pun, B. He, J. Yang, F. M. Toma, I. D. Sharp, O. M. Yaghi, J. Fan, S. -R. Zheng, W. -G. Zhang, Y. Liu. *Chem. Sci.* **2014**, *5*, 4693.

[139] M. Bendikov, F. Wudl. *Chem. Rev*. **2004**, *104*, 4891.

[140] J. Xiao, Z. Yin, H. Li, Q. Zhang, F. Boey, H. Zhang, Q. Zhang. *J. Am. Chem. Soc.* **2010**, *132*, 6926.

[141] S. Jin, T. Sakurai, T. Kowalczyk, S. Dalapati, F. Xu, H. Wei, X. Chen, J. Gao, S. Seki, S. Irle, D. Jiang. *Chem. Eur. J.* **2014**, *20*, 14608.

[142] H. Ding, Y. Li, H. Hu, Y. Sun, J. Wang, C. Wang, C. Wang, G. Zhang, B. Wang, W. Xu, D. Zhang. *Chem. Eur. J.* **2014**, *20*, 14614.

[143] P. H. Qi, J. B. Hiskey. *Hydrometallurgy* **1993**, *32*, 161.

[144] D. Jérome. *Chem. Rev.* **2004**, *104*, 5565.

[145] S. S. Park, E. R. Hontz, L.Sun, C. H. Hendon, A. Walsh, T. V. Voorhis, M. Dincă. *J. Am. Chem. Soc.* **2015**, *137*, 1774.

[146] J. Su, S. Yuan, H. -Y. Wang, L. Huang, J. -Y. Ge, E. Joseph, J. Qin, T. Cagin, J. -L. Zuo, H. -C. Zhou. *Nat. Commun.* **2017**, *8*, 2008.

[147] L. Sun, S. S. Park, D. Sheberla, and M. Dincă. *J. Am. Chem. Soc.* **2016**, *138*, 14772.

[148] E. Jin, M. Asada, Q. Xu, S. Dalapati, M. A. Addicoat, M. A. Brady, H. Xu, T. Nakamura, T. Heine, Q. Chen, D. Jiang. *Science* **2017**, *357*, 673.

[149] Y. Wu, D. Yan, Z. Zhang, M. M. Matsushita, K. Awaga. *ACS Appl. Mater. Interfaces* **2019**, *11*, 7661.

[150] I. Stassen, N. Burtch, A. Talin, P. Falcaro, M. Allendorf, R. Ameloot. *Chem. Soc. Rev.* **2017**, *46*, 3185.

[151] S. Mohanapriya, S. D. Bhat, A. K. Sahu, S. Pitchumani, P. Sridhar, A. K. Shukla.

Energy Environ. Sci. **2009**, *2*, 1210.

[152] J. C. Bachman, S. Muy, A. Grimaud, H. -H. Chang, N. Pour, S. F. Lux, O. Paschos, F. Maglia, S. Lupart, P. Lamp, L. Giordano, Y. Shao-Horn. *Chem. Rev.* **2016**, *116*, 140.

[153] M. A. Hickner, H. Ghassemi, Y. S. Kim, B. R. Einsla, J. E. McGrath. *Chem. Rev.* **2004**, *104*, 4587.

[154] T. Higashihara, K. Matsumoto, M. Ueda. *Polymer* **2009**, *50*, 5341.

[155] J. A. Mader, B. C. Benicewicz, *Macromolecules* **2010**, *43*, 6706.

[156] S. Horike, D. Umeyama, S. Kitagawa. *Acc. Chem. Res.* **2013**, *46*, 2376.

[157] G. K. H. Shimizu, J. M. Taylor, S. Kim. *Science* **2013**, *341*, 354.

[158] J. Jiang, Y. Zhao, O. M. Yaghi. *J. Am. Chem. Soc.* **2016**, *138*, 3255.

[159] S. Bureekaew, S. Horike, M. Higuchi, M. Mizuno, T. Kawamura, D. Tanaka, N. Yanai, S. Kitagawa. *Nat. Mater*. **2009**, *8*, 831.

[160] J. A. Hurd, R. Vaidhyanathan, V. Thangadurai, C. I. Ratcliffe, I. L. Moudrakovski, G. K. H. Shimizu. *Nat. Chem.* **2009**, *1*, 705.

[161] D. E. Katsoulis. *Chem. Rev.* **1998**, *98*, 359.

[162] H. N. Miras, L. Vilà-Nadal, L. Cronin. *Chem. Soc. Rev.* **2014**, *43*, 5679.

[163] H. Ma, B. Liu, B. Li, L. Zhang, Y.-G. Li, H. -Q. Tan, H. -Y.Zang, G. Zhu. *J. Am. Chem. Soc*. **2016**, *138*, 5897.

[164] H. Xu, S. Tao, D. Jiang,*Nat. Mater.* **2016**, *15*, 722.

[165] H. S. Sasmal, H. B. Aiyappa, S. N. Bhange, S. Karak, A. Halder, S. Kurungot, R. Banerjee *Angew. Chem. Int. Ed.* **2018**, *57*, 10894.

[166] M. Park, X. Zhang, M. Chung, G. B. Less, A. M. Sastry. *J. Power Sources* **2010**, *195*, 7904.

[167] B. F. Abrahams, D. J. Price, R. Robson. *Angew. Chem. Int. Ed.* **2006**, *45*, 806.

[168] Y. Zhang, J. Duan, D. Ma, P. Li, S. Li, H. Li, J. Zhou, X. Ma, X. Feng, B. Wang. *Angew. Chem. Int. Ed.* **2017**, *56*, 16313.

[169] Y. Hu, N. Dunlap, S. Wan, S. Lu, S. Huang, I. Sellinger, M. Ortiz, Y. Jin, S. -H. Lee, W. Zhang. *J. Am. Chem. Soc.* **2019**, *141*, 7518.

[170] T. J. Barbarich, P. F. Driscoll, S. Izquierdo, L. N. Zakharov, C. D. Incarvito, A. L. Rheingold. *Inorg. Chem.* **2004**, *43*, 7764.

[171] K. Jeong, S. Park, G. Y. Jung, S. H. Kim, Y. -H. Lee, S. K. Kwak, S. -Y. Lee. *J. Am. Chem. Soc.* **2019**, *141*, 5880.

[172] F. Croce, G. B. Appetecchi, L. Persi, B. Scrosati. *Nature* **1998**, *394*, 456.

[173] Z. Gadjourova, Y. G. Andreev, D. P. Tunstall, P. G. Bruce. *Nature* **2001**, *412*, 520.

[174] R. Khurana, J. L. Schaefer, L. A. Archer, G. W. Coates, *J. Am. Chem. Soc.* **2014**, *136*, 7395.

[175] Q. Xu, S. Tao, Q. Jiang, D. Jiang. *J. Am. Chem. Soc.* **2018**, *140*, 7429.

[176] H. Xu, J. Gao, D. Jiang. *Nat. Chem.* **2015**, *7*, 905.

[177] Q. Xu, S. Tao, Q. Jiang, D. Jiang. *Angew. Chem. Int. Ed.* **2020**, doi: 10.1002/anie.201915234.

[178] Z. Guo, Y. Zhang, Y. Dong, J. Li, S. Li, P. Shao, X. Feng, B. Wang. *J. Am. Chem. Soc.* **2019**, *141*, 1923.

[179] Z. Xie, B. Wang, Z. Yang, X. Yang, X. Yu, G. Xing, Y. Zhang, L. Chen. *Angew. Chem. Int. Ed.* **2019**, *58*, 15742.

[180] N. Armaroli, V. Balzani, *Angew. Chem. Int. Ed.* 2007, **46**, 52.

[181] W. Lubitz, B. Tumas, *Chem. Rev.* **2007**, *107*, 3900.

[182] U. Eberle, M. Felderhoff, F. Schüth. *Angew. Chem. Int. Ed.* **2009**, *48*, 6608.

[183] M. Z. Jacobson, W. G. Colella, D. M. Golden, *Science* 2005, **308**, 1901.

[184] H. Wang, Z. Zeng, P. Xu, L. Li, G. Zeng, R. Xiao, Z. Tang, D. Huang, L. Tang, C. Lai, D. Jiang, Y. Liu, H. Yi, L. Qin, S. Ye, X. Rena,W. Tang. *Chem. Soc. Rev.* **2019**, *48*, 488.

[185] A. P. Ruigõmez, D. Rodríguez-San-Miguel, K. C. Stylianou, M. Cavallini, D. Gentili,

F. Liscio, S. Milita, O. M. Roscioni, M. L. Ruiz-González, C. Carbonell, D. Maspoch, R. Mas-Ballesté, J. L. Segura, F. Zamora. *Chem. Eur. J.* **2015**, *21*, 10666.

[186] C. Montoro, D. Rodríguez-San-Miguel, E. Polo, R. Escudero-Cid, M. L. Ruiz-González, J. A. R. Navarro, P. Ocón, F. Zamora. *J. Am. Chem. Soc.* **2017**, *139*, 10079.

[187] L. C. Tabares, J. A. R. Navarro, J. M. Salas. *J. Am. Chem. Soc.* **2001**, *123*, 383.

[188] X. Meng, H. -N. Wang, S. -Y. Song, and H. -J. Zhang, *Chem. Soc. Rev.* **2017**, *46*, 464.

[189] D. W. Kang, K. S. Lim, K. J. Lee, J. H. Lee, W. R. Lee, J. H. Song, K. H. Yeom, J. Y. Kim, C. S. Hong. *Angew. Chem. Int. Ed.* **2016**, ***55***, 16123.

[190] D. B. Shinde, H. B. Aiyappa, M. Bhadra, B. P. Biswal, P. Wadge, S. Kandambeth, B. Garai, T. Kundu, S. Kurungot, R. Banerjee. *J. Mater. Chem. A* **2016**, *4*, 2682.

[191] Y. Yin, Z. Li, X. Yang, L. Cao, C. Wang, B. Zhang, H. Wu, Z. Jiang. *J. Power Sources* **2016**, *332*, 265.

[192] H. Jin, C. Guo, X. Liu, J. Liu, A. Vasileff, Y. Jiao, Y. Zheng, S. -Z. Qiao. *Chem. Rev.* **2018**, *118*, 6337.

[193] N. -T. Suen, S. -F. Hung, Q. Quan, N. Zhang, Y. -J. Xu, H. M. Chen. *Chem. Soc. Rev.* **2017**, *46*, 337.

[194] H. -F. Wang, L. Chen, H. Pang, S. Kaskel, Q. Xu. *Chem. Soc. Rev.* **2020**, doi: 10.1039/c9cs00906j.

[195] V. R. Stamenkovic, D. Strmcnik, P. P. Lopes, N. M. Markovic. *Nat. Mater.* **2017**, *16*, 57.

[196] Y. Yan, T. He, B. Zhao, K. Qi, H. Liu, B. Y. Xia. *J. Mater. Chem. A* **2018**, *6*, 15905.

[197] S. Cao, B. Li, R. Zhu, H. Pang. *Chem. Eng. J.* 2018, **355**, 602.

[198] H. Hu, Q. Yan, R. Ge, Y. Gao. *Chinese J. Catal.* **2018**, *39*, 1167.

[199] J. Qiao, Y. Liu, F. Hong, J. Zhang. *Chem. Soc. Rev.* **2014**, *43*, 631.

[200] D. Behar, T. Dhanasekaran, P. Neta, C. M. Hosten, D. Ejeh, P. Hambrightand, E. Fujita. J. *Phys. Chem. A* **1998**, *102*, 2870.

[201] C. S. Diercks, S. Lin, N. Kornienko, E. A. Kapustin, E. M. Nichols, C. Zhu, Y. Zhao, C. J. Chang, O. M. Yaghi. *J. Am. Chem. Soc.* **2018**, *140*, 1116.

[202] H.-J. Zhu, M. Lu, Y. -R. Wang, S. -J. Yao, M. Zhang, Y. -H. Kan, J. Liu, Y. Chen, S. -L. Li, Y. -Q. Lan. *Nat. Commun.* **2020**, *11*, 497.

[203] T. C. Narayan, T. Miyakai, S. Seki, M. Dincă. *J. Am. Chem. Soc.* **2012**, *134*, 12932.

[204] S. Wan, F. Gándara, A. Asano, H. Furukawa, A. Saeki, S. K. Dey, L. Liao, M. W. Ambrogio, Y. Y. Botros, X. Duan, S. Seki, J. F. Stoddart, O. M. Yaghi. *Chem. Mater.* **2011**, *23*, 4094.

[205] H. Liu, J. Chu, Z. Yin, X. Cai, L. Zhuang, H. Deng. *Chem* **2018**, *4*, 1696.

[206] B. E. Logan, B. Hamelers, R. Rozendal, U. SchröDer, J. Keller, S. Freguia, P. Aelterman, W. Verstraete, K. Rabaey. *Environ. Sci. Technol.* **2006**, *40*, 5181.

[207] A. A. Gewirth, M. S. Thorum. *Inorg. Chem.* **2010**, *49*, 3557.

[208] S. Royuela, E. Martínez-Periñán, M. P. Arrieta, J. I. Martínez, M. M. Ramos, F. Zamora, E. Lorenzo, J. L. Segura, *Chem. Commun.* **2020**, *56*, 1267.

[209] E. Castaldelli, E. R. Triboni, G. J. -F. Demets. *Chem. Commun.* **2011**, *47*, 5581.

[210] K. Kamiya, R. Kamai, K. Hashimoto, S. Nakanishi. *Nat. Commun.* **2014**, *5*, 5040.

[211] K. Iwase, T. Yoshioka, S. Nakanishi, K. Hashimoto, K. Kamiya. *Angew. Chem. Int. Ed.* **2015**, *54*, 11068.

[212] C. Hu, L. Zhang, J. Gong. *Energy Environ. Sci.* **2019**, *12*, 2620.

[213] H. B. Aiyappa, J. Thote, D. B. Shinde, R. Banerjee, and S. Kurungot. *Chem. Mater.* **2016**, *28*, 4375.

[214] S. Pintado, S. Goberna-Ferrón, E. C. Escudero-Adán, J. L. Galán-Mascarós. J. *Am. Chem. Soc.* **2013**, *135*, 13270.

[215] Y. Surendranath, M. Dincă, D. G. Nocera. J. *Am. Chem. Soc.* **2009**, *131*, 2615.

[216] X. Zhao, P. Pachfule, S. Li, T. Langenhahn, M. Ye, C. Schlesiger, S. Praetz, J. Schmidt, A. Thomas. *J. Am. Chem. Soc.* **2019**, *141*, 6623.

[217] C. Yang, Z. -D. Yang, H. Dong, N. Sun, Y. Lu, F. -M. Zhang, G. Zhang. *ACS Energy Lett.* **2019**, *4*, 2251.

[218] S. Dalapati, E. Jin, M. Addicoat, T. Heine, D. Jiang, *J. Am. Chem. Soc.* **2016**, *138*, 5797.

[219] S. Bhunia, S. K. Das, R. Jana, S. C. Peter, S. Bhattacharya, M. Addicoat, A. Bhaumik, A. Pradhan. *ACS Appl. Mater. Interfaces* **2017**, *28*, 23843.

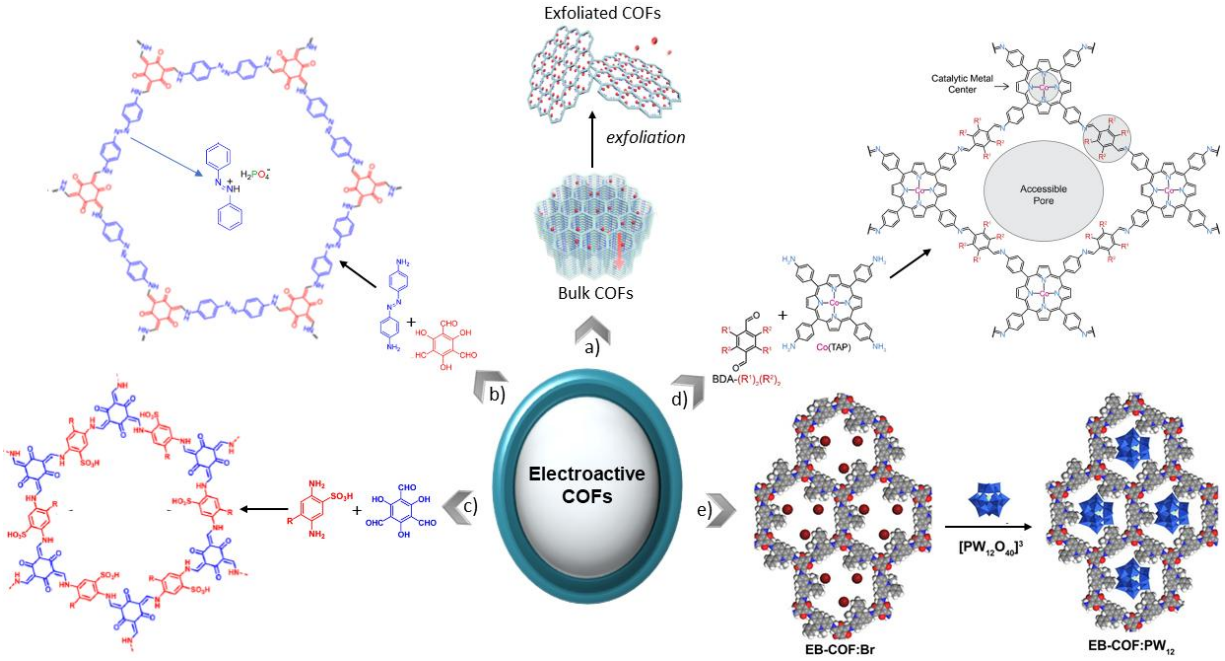

Scheme 1. General design of electroactive COFs. a) Typical design of electroactive bulk COFs and exfoliated COFs. Reproduced with permission.[46] Copyright 2017, American Chemical Society. b) Typical bottom-up design of electroactive COFs with reactive skeletons. Reproduced with permission.[47] Copyright 2014, American Chemical Society. c) Typical bottom-up design of electroactive COFs with reactive functional groups. Reproduced with permission.[54] Copyright 2016, American Chemical Society. d) Typical bottom-up design of electroactive COFs with reactive metals. Reproduced with permission.[199] Copyright 2018, American Chemical Society. e) Typical design of electroactive COF hybrids. Reproduced with permission.[162] Copyright 2016, American Chemical Society.

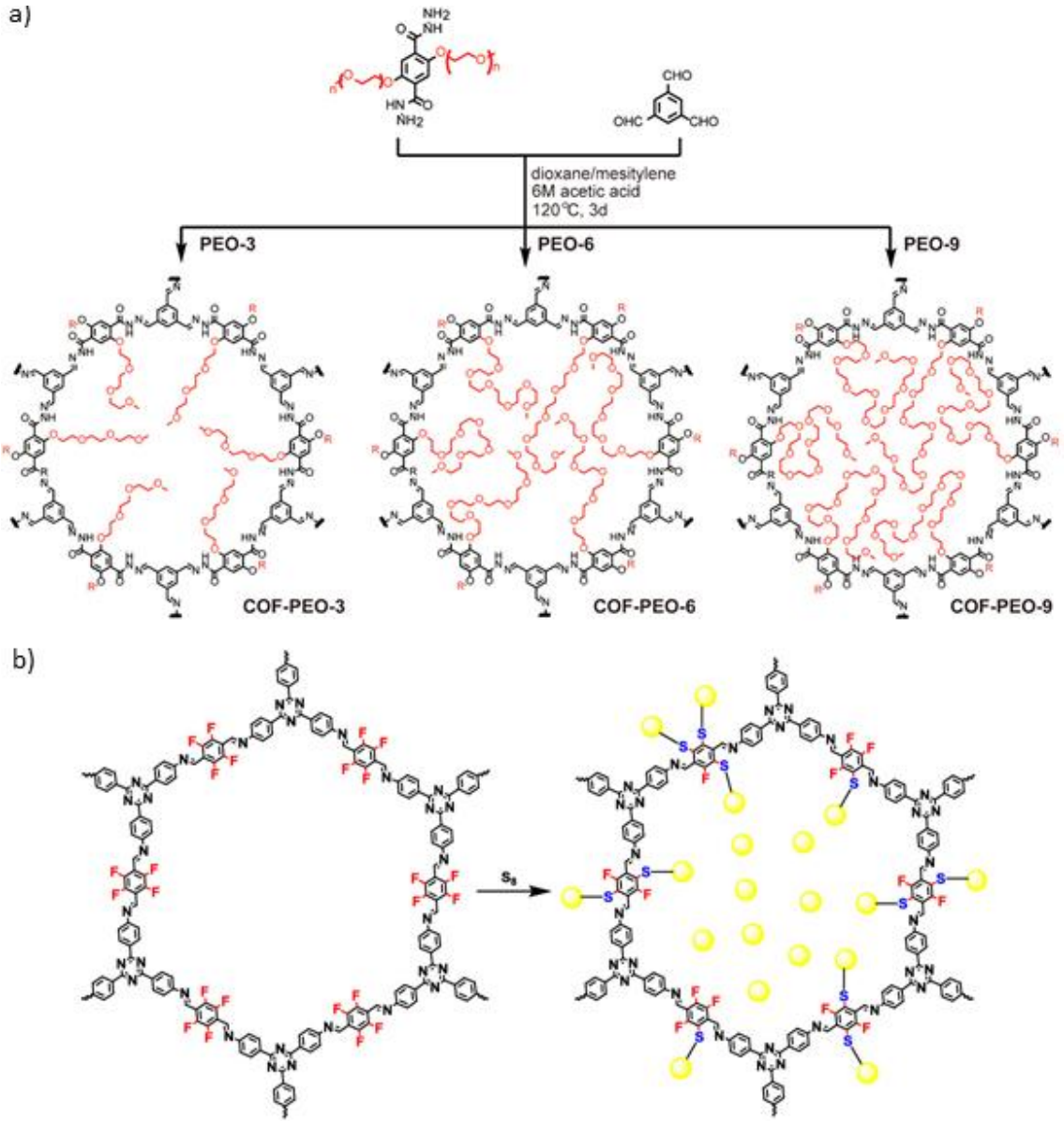

Figure 1. Design of COFs with electroactive functional groups. a) Bottom-up design of COF-PEO-*x* series by condensing PEO-based building units. Reproduced with permission.[55] Copyright 2019, American Chemical Society. b) Design of COF-F-S by postsynthetically chemically modifying the pre-established COF-F with elemental polysulfur (PS). Reproduced with permission.[41] Copyright 2018, American Chemical Society.

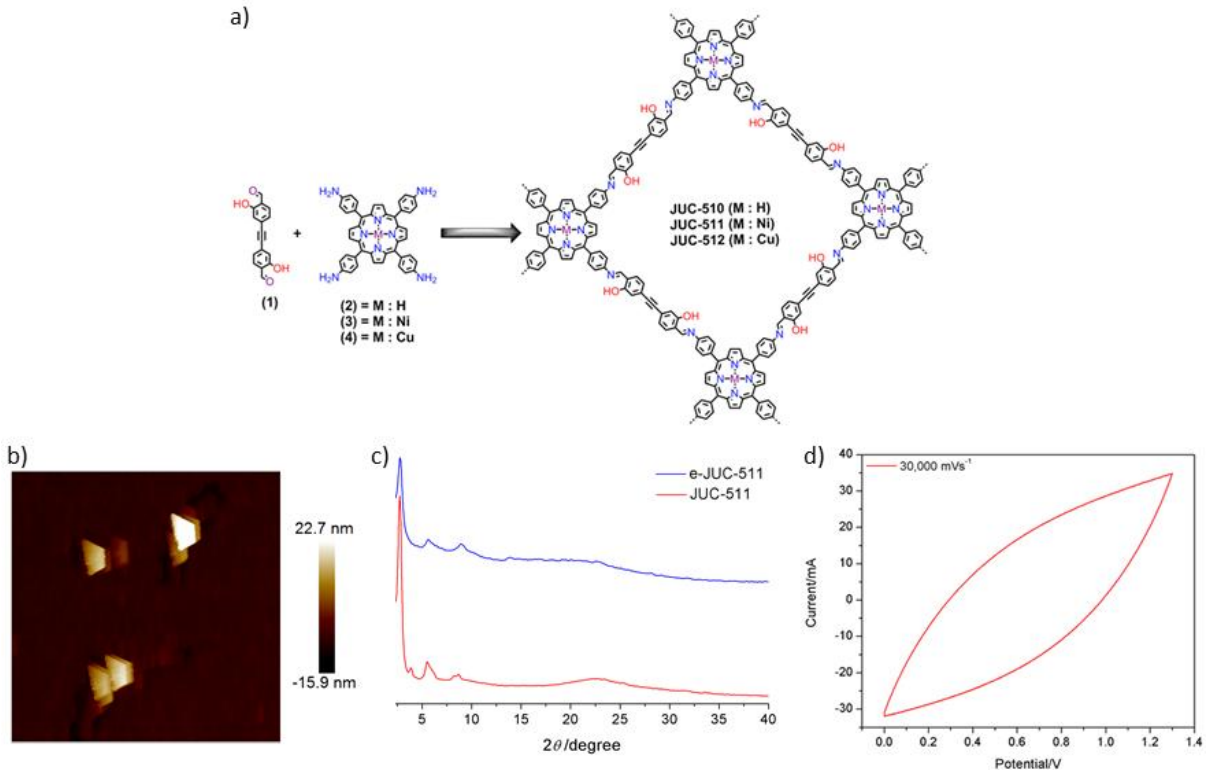

Figure 2. Structural and electrochemical analyzes of e-COF based EDLCs. a) Designed synthesis of mesoporous JUC-COFs. b) AFM image of e-COF with maximum layer thickness of ≈ 22 nm. c) PXRD patterns of e-COF and COF. d) CV curve of e-COF capacitor cell at high scan rate of 30,000 mV s^{-1}. Reproduced with permission.[34] Copyright 2020, Wiley-VCH.

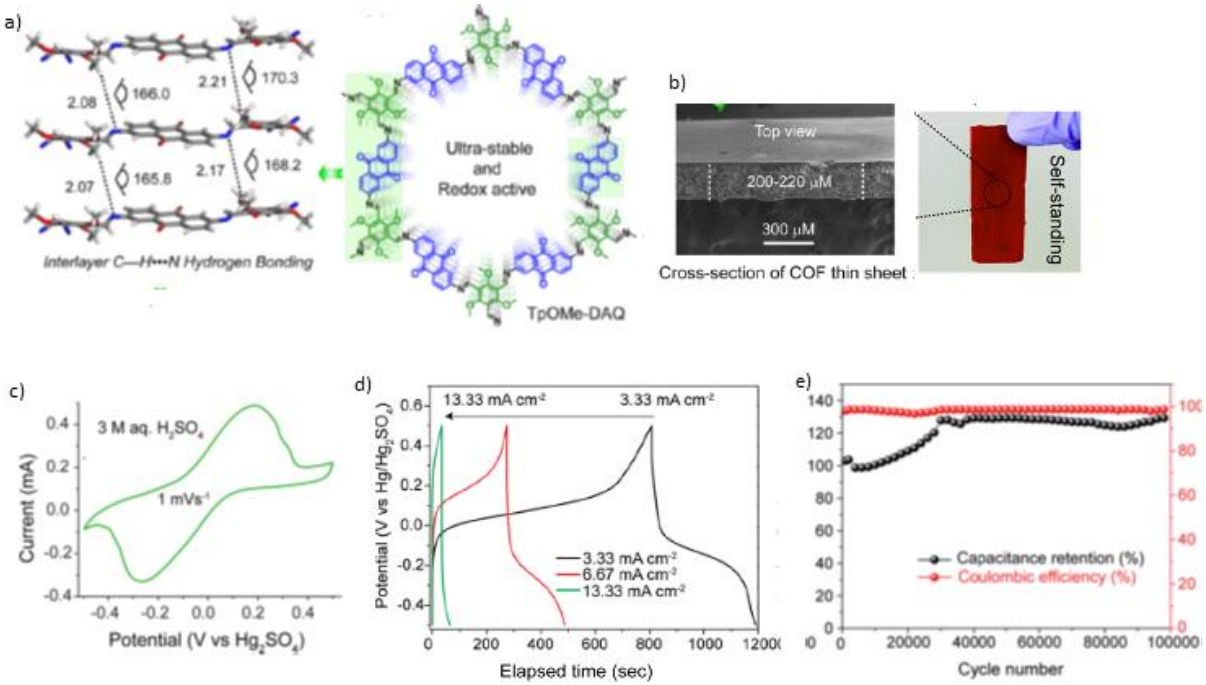

Figure 3. The electrochemical analysis of self-standing electrode based TpOMe-DAQ. a) Layer structure of TpOMe-DAQ depicting interlayer H-bonding. b) Self-standing nature of TpOMe-DAQ with average thickness of ~ 200 μm. c) CV curve of TpOMe-DAQ electrode in 3 M H_2SO_4 at scan rate of 1 mV s^{-1}. d) GCD curves of TpOMe-DAQ with 7.5 mm^2 active area. e) Cyclic stability performance of TpOMe-DAQ electrode (at 10 mA cm^{-2}). Reproduced with permission.[40] Copyright 2018, American Chemical Society.

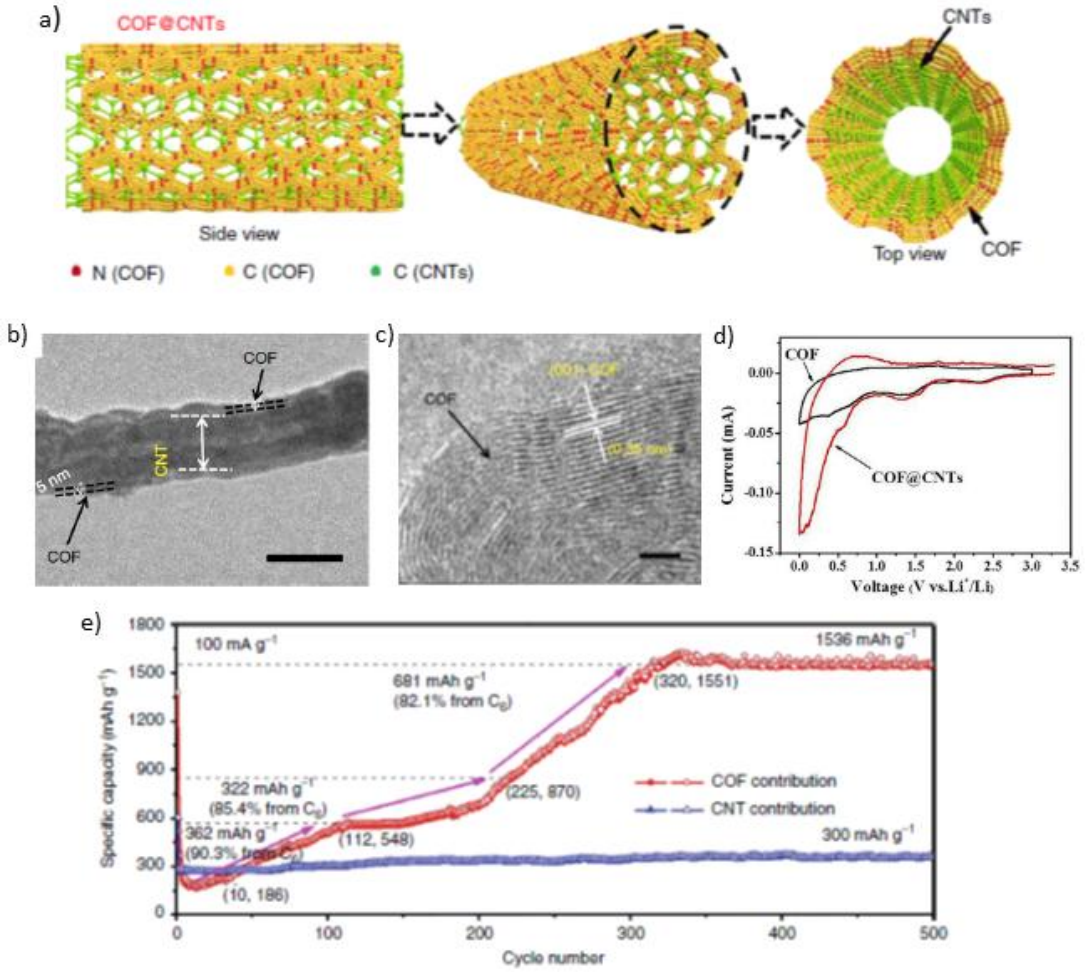

Figure 4. The synthesis of electrochemical behavior of COF@CNTs as LIB anodes. a) Graphical representation of COF@CNTs with few COF layers covered on the exterior surface of CNTs. b-c) TEM images of COF@CNTs. Scale bar, 100 nm. d) CV curves of the COF@CNTs and COF anodes measured at 0.1 mV s^{-1} (at first-cycle; between 3.25 V and 0.5 mV). e) Capacity contribution of COF (based on the mass of COF) in COF@CNTs at 100 mA g^{-1}. Reproduced with permission under Creative Commons CC BY license.[67] Copyright 2018, Nature Publishing Group.

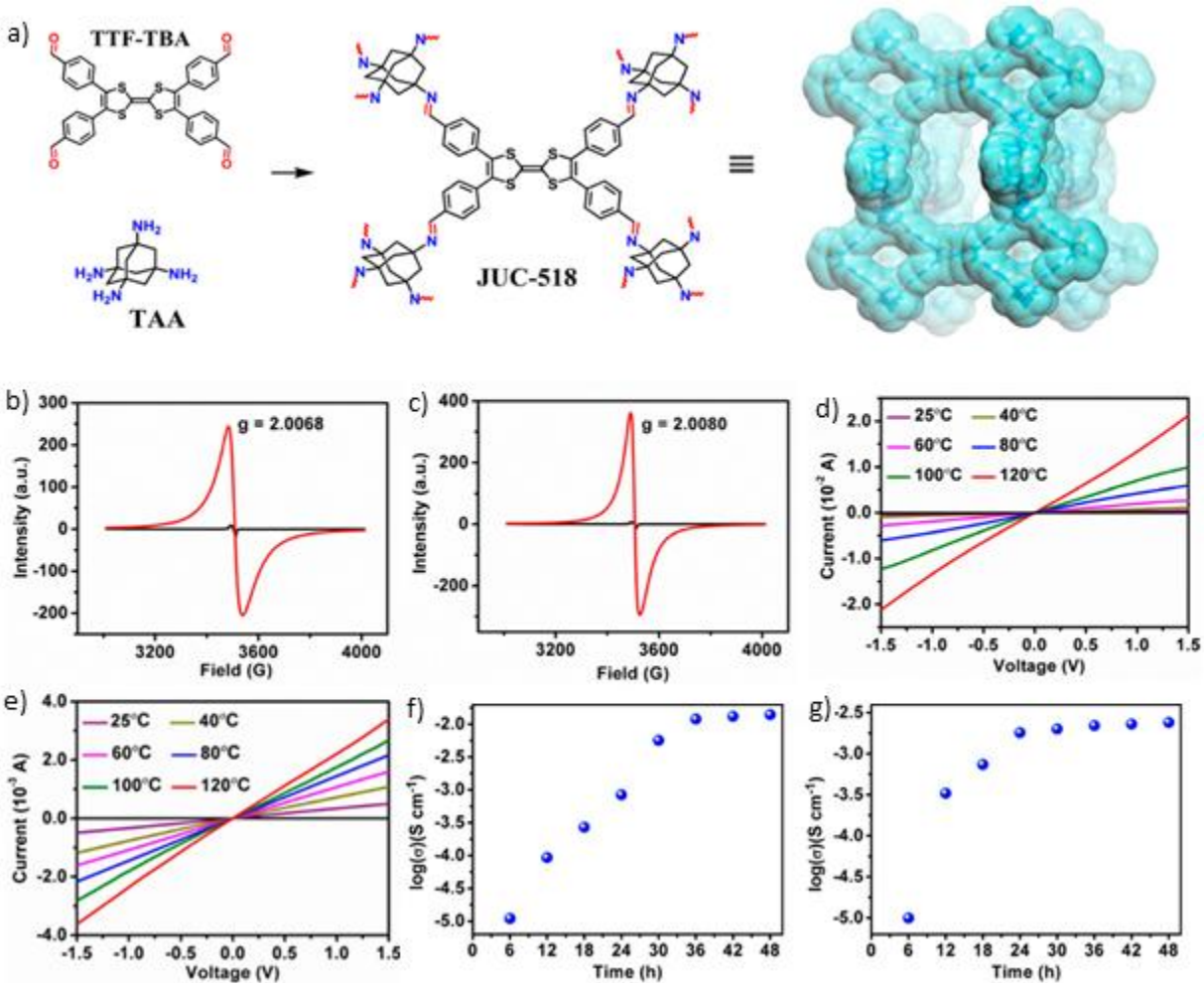

Figure 5. The synthesis and electrical conductivity analysis of 3D-TTF-COFs. a) Design synthesis of JUC-518 and its 3D extended structure. b-c) Solid-state EPR spectra of JUC-518 and JUC-519. d-e) Temperature-dependent *I*–*V* curves of JUC-518 and JUC-519 upon doping with I_2. f-g) Time-dependent electrical conductivities of JUC-518 and JUC-519 upon doping with I_2. Reproduced with permission.[35] Copyright 2019, American Chemical Society.

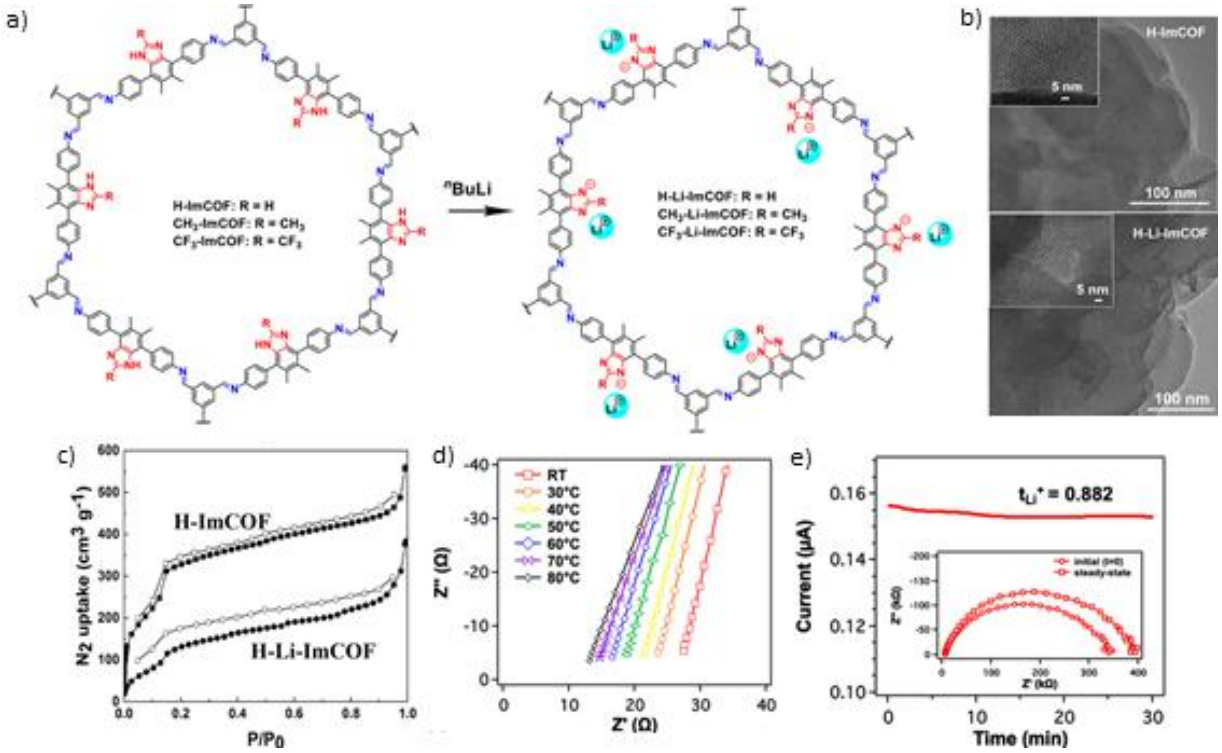

Figure 6. The synthesis and lithium conductivity analysis of R-Li-ImCOFs. a) The synthesis of R-Li-ImCOFs from lithiation of R-ImCOFs. b) TEM images of H-ImCOF and H-Li-ImCOF indicating the retained of the crystallinity of both materials. c) The N_2 adsorption−desorption isotherms of H-ImCOF and H-Li-ImCOF. c) Nyquist plots of EIS measurements of H-Li-ImCOF at different temperatures. d) the t_{Li^+} plot of H-Li-ImCOF calculated using the Bruce− Vincent−Evans technique. Reproduced with permission.[167] Copyright 2019, American chemical Society.

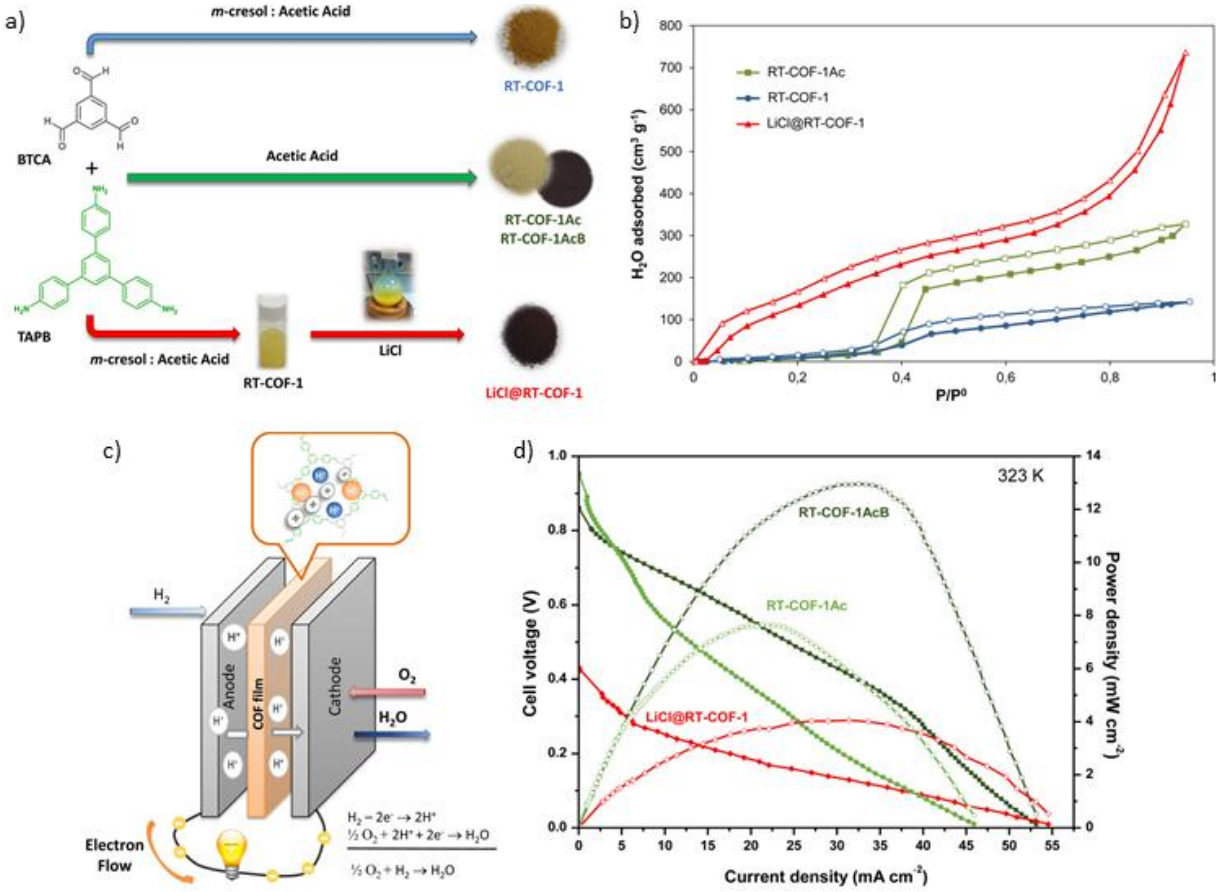

Figure 7. The synthesis and the application of RT-CO-1 series in proton exchange membrane (PEM) fuel cells. a) Schematic representation of the synthesis of RT-COF-1, RT-COF-1Ac, RT-COF-1AcB, and LiCl@RT-COF-1. b) Water vapor adsorption isotherms of RT-COF-1, RT-COF-1Ac, and LiCl@RT-COF-1 (at 298 K). c) Scheme of the PEMFC composed of RT-COF-1Ac, RT-COF- 1AcB, and LiCl@RT-COF-1 films as membrane electrode assemblies (MEA). d) Polarization (filled symbols) and power density (open symbols) curves of RT-COF-1Ac, RT-COF-1AcB, and LiCl@RT-COF-1 films measured at 323 K for a single H_2/O_2 PEMFC. Reproduced with permission.[184] Copyright 2017, American Chemical Society.

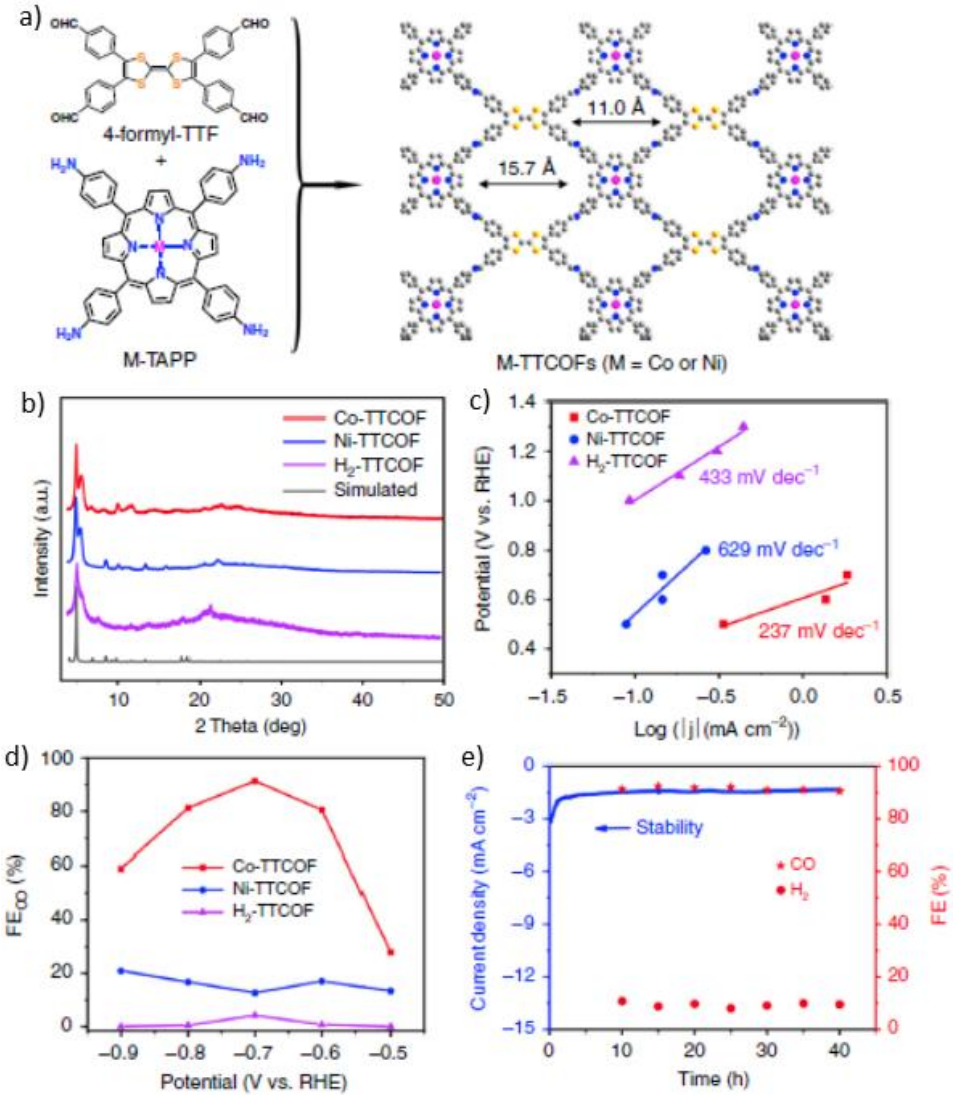

Figure 8. The synthesis and electrocatalytic performance of M-TTCOFs towards reduction of CO_2. a) Design synthesis of M-TTCOFs (M = Co or Ni). b) PXRD patterns of M-TTCOFs. c) Tafel plots of M-TTCOFs. d) The FE_{CO} curve of M-TTCOFs calculated over potential range −0.5 to −0.9 V. e) Cycling stability test of Co-TTCOF at the potential of −0.7 V *vs.* RHE. Reproduced with permission under Creative Commons CC BY license.[200] Copyright 2020, Nature Publishing Group.

Author Biographies

Yusran Yusran received his B.Sc. (2012) degree in Chemistry with honors from State University of Makassar, Indonesia and M.Sc. (2014) degree in chemistry from Gadjah Mada University (UGM), Yogjakarta Indonesia. He then attended State Key Laboratory of Inorganic Synthesis and Preparative Chemistry, Jilin University, China, as research student working on metal organic frameworks (MOFs). From 2016 till present he has been a Ph.D student in the same lab under supervision of Prof. Qianrong Fang and Prof. Shilun Qiu. His current research focus on porous materials including MOFs and covalent organic frameworksc (COFs) and their potential applications in catalysis and energy storage.

Qianrong Fang obtained his B.S. (2001) and Ph.D (2007) degrees in Chemistry from Jilin University in China. From 2007 to 2014, he completed his postdoctoctoral study in University of California at Los Angeles, Texas A&M University, University of California at Riverside as well as University of Delaware. In 2015, he received 1000 Young Talent Plan of China and went back to the State Key Laboratory of Inorganic Synthesis & Preparative Chemistry at Jilin University, as a full professor. His current research focuses on the design and synthesis of covalent organic frameworks (COFs) for applications in adsorption, separation, catalysis, and a number of others.

Valentin Valtchev studied Geochemistry at the University of Sofia and completed his Ph.D. in 1991 at the Bulgarian Academy of Sciences. He has worked as postdoctoral research fellow in the groups of Prof. Alan Dyer (1992–1993) and Prof. Johan Sterte (1995–1996). In 1996, he was promoted to Senior Researcher at the Bulgarian Academy of Sciences. He joined the Laboratory of Inorganic Materials, University of Haute Alsace (UHA), Mulhouse, France as Research Associate during 2000–2006. Since 2006 till present, he has been appointed as a CNRS Research Director and Head of the Materials Science Group at the Laboratory of Catalysis and Spectroscopy in Caen. His research involves the synthesis, characterization, and modification of microporous materials, such as zeolites and other porous solids that can be used for catalysis, separation, and molecular recognition.

The table of contents entry:

The design synthesis and applications of electroactive covalent organic frameworks (COFs) are summarized. Significant progresses have been made in the design and application of electroactive COFs in the field of capacitors, batteries, conductors, fuel-cells, and electrocatalysis. Their remarkable performances are discussed and compared with other porous materials, while prespectives in development of electroactive COFs are also provided.

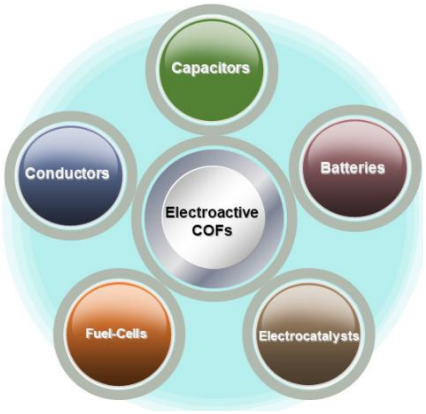
Capacitors
Conductors
Batteries
Electroactive COFs
Fuel-Cells
Electrocatalysts